

Chapter 19

Tracking Detectors

19.1 Physics Goals

The primary physics goal of the tracking detectors is to measure the muon beam profile at multiple locations around the ring as a function of time throughout the muon fill. This information will be used to determine several parameters associated with the dynamics of the stored muon beam [1]. This is required for the following reasons:

- Momentum spread and betatron motion of the beam lead to ppm level corrections to the muon precession frequency associated with the fraction of muons that differ from the magic momentum and the fraction of time muons are not perpendicular to the storage ring field.
- Betatron motion of the beam causes acceptance changes in the calorimeters that must be included in the fitting functions used to extract the precession frequency.
- The muon spatial distribution must be convoluted with the measured magnetic field map in the storage region to determine the effective field seen by the muon beam.

The secondary physics goal of the tracking detectors involves understanding systematic uncertainties associated with the muon precession frequency measurement derived from calorimeter data. In particular, the tracking system will isolate time windows that have multiple positrons hitting the calorimeter within a short time period and will provide an independent measurement of the momentum of the incident particle. This will allow an independent validation of techniques used to determine systematic uncertainties associated with calorimeter pileup, calorimeter gain, and muon loss based solely on calorimeter data.

The tertiary physics goal of the tracking detectors is to determine if there is any tilt in the muon precession plane away from the vertical orientation. This would be indicative of a radial or longitudinal component of the storage ring magnetic field or a permanent electric dipole moment (EDM) of the muon [2]. Any of these effects directly biases the precession frequency measurement. A tilt in the precession plane leads to an up-down asymmetry in the positron angle that can only be measured with the tracking detectors. The goals for the systematic uncertainties that can be directly determined or partially constrained using tracking information are listed in Table 19.1.

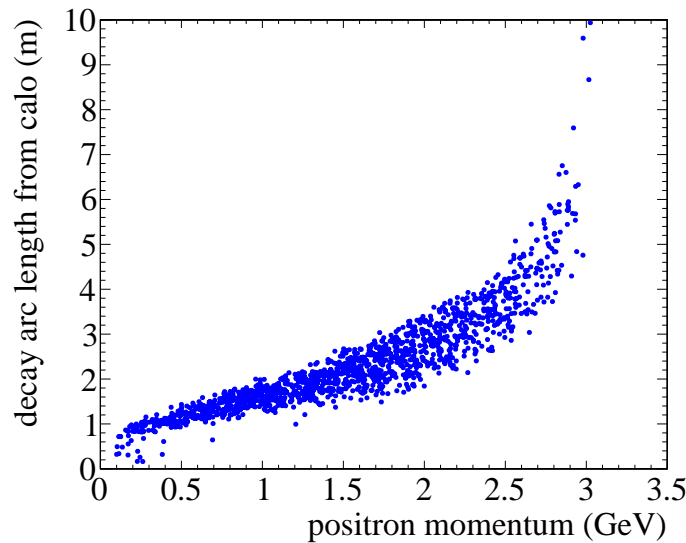


Figure 19.1: Arc length between the calorimeter and the muon decay point as a function of positron momentum.

Uncertainty	E821 value	E989 goal	Role of tracking
Magnetic field	0.03 ppm	0.01 ppm	Measure beam profile on a fill by fill basis ensuring proper muon beam alignment
Beam dynamics corrections	0.05 ppm	0.03 ppm	Measure beam oscillation parameters as a function of time in the fill
Pileup correction	0.08 ppm	0.04 ppm	Isolate time windows with more than one positron hitting the calorimeter to verify calorimeter based pileup correction
Calorimeter gain stability	0.12 ppm	0.02 ppm	Measure positron momentum with better resolution than the calorimeter to verify calorimeter based gain measurement
Precession plane tilt	4.4 μ Rad	0.4 μ Rad	Measure up-down asymmetry in positron decay angle

Table 19.1: Systematic uncertainty goals for the Muon g-2 experiment. Information from the tracking detectors will be used to constrain these in several ways as indicated in the final column. The first two rows are associated with the tracker’s primary physics goal. The second two are associated with the secondary physics goal of the tracker and the main role played by the tracker will be in validating the reductions in the uncertainties provided by the new calorimeters. The final row is associated with the tertiary physics goal and the improvements are entirely from increased acceptance and statistics in the new experiment.

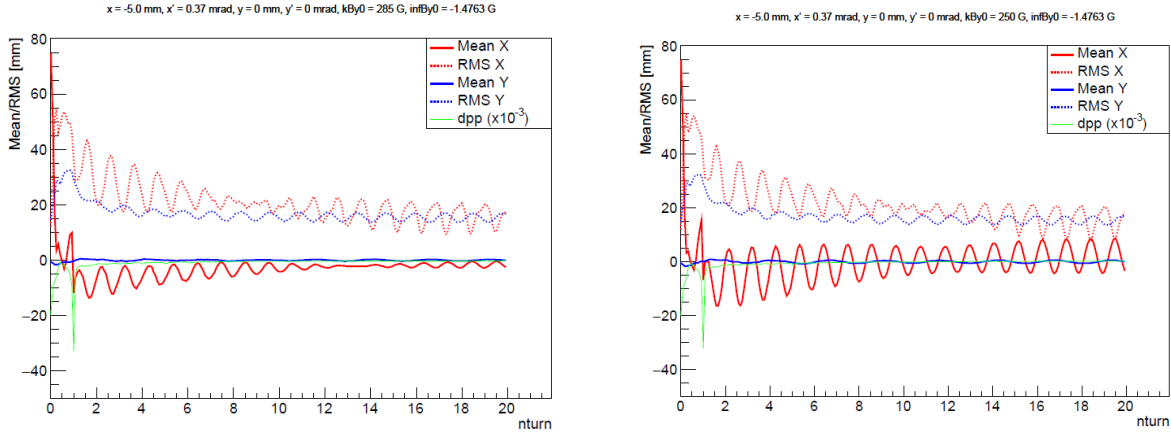


Figure 19.2: The beam position and width for optimal and sub-optimal injection parameters. The solid rd line is the horizontal mean. The dashed red line is the horizontal width. The solid blue line is the vertical mean. The dashed blue line is the vertical width. The green line is the momentum spread of the beam. The distributions demonstrate the need to measure beam positions near millimeter level accuracy.

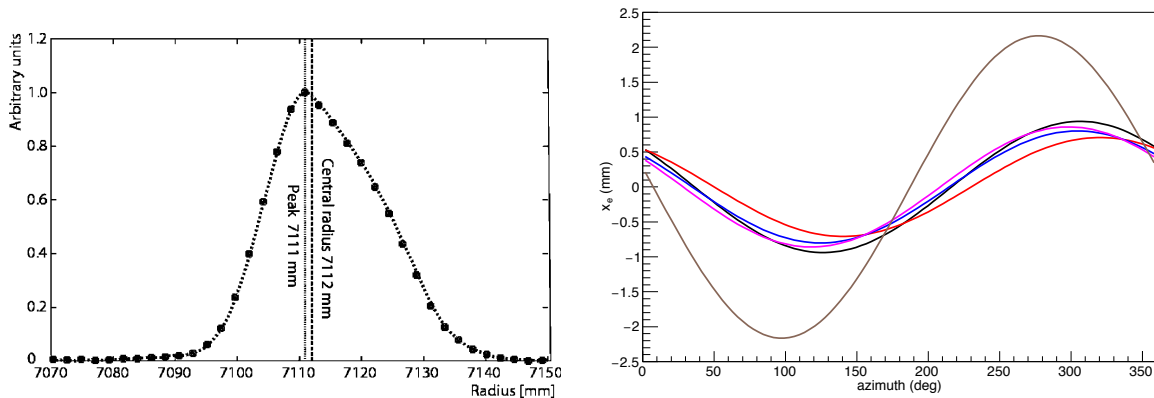


Figure 19.3: Left: The distribution of equilibrium radii measured in the Brookhaven experiment reproduced from Ref. [1]. Right: The equilibrium radius as a function of azimuth around the ring inferred from the non-uniformities in the measured field map for five different trolley runs. The distributions demonstrate the need for millimeter level accuracy and the need for multiple position measurements around the ring.

19.2 Requirements

The DC nature of the muon beam requires that the tracker perform well over a large momentum range and for muon decay positions up to 10 meters in front of the first tracking plane. The arc length between the calorimeter and the muon decay point as a function of positron momentum is shown in Fig. 19.1.

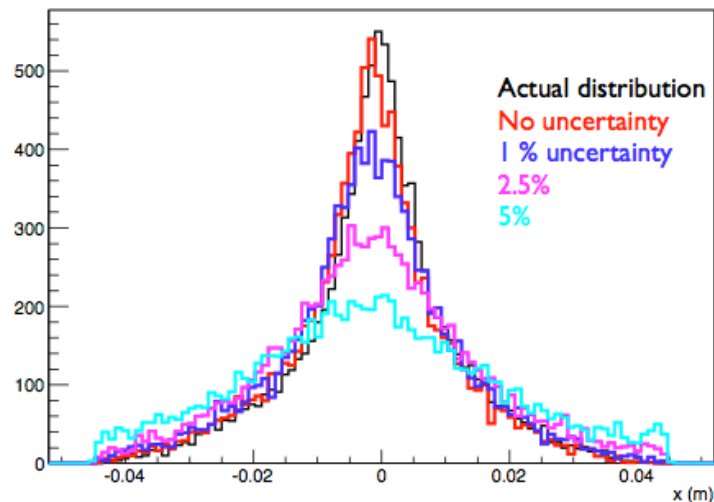


Figure 19.4: The reconstructed beam distribution in the radial dimension for several different assumed uncertainties on the reconstructed curvature of the positron track. A resolution at or below 1% is desirable to reconstruct both the beam mean and width.

The expected change in the radial beam center and width due to betatron oscillations as predicted by the BMAD simulation is shown in Fig. 19.2. The position oscillates with an amplitude of approximately 4 mm and the width oscillates with an amplitude of roughly 2 mm. A measurement with mm level resolution is required to map out this motion. Since the beam has non-integer tune, these features can be seen by a single tracker however, a second measurement position is required for cross checking and redundancy.

The equilibrium radius of the E821 beam is shown in Fig. 19.3. The beam was shifted from the central orbit by roughly 1 mm. Figure 19.3 also shows the equilibrium radii of the E821 beam as a function of position around the ring inferred from the magnetic field measurements. These two distributions also indicate that mm level precision is required. The change in the radii as a function of position around the ring can not be measured by a single tracking station and requires maximizing the number of measurement locations.

Figure 19.4 shows the results of track reconstruction code applied to the BMAD simulation for different values of the momentum resolution of the reconstructed helix. One sees that percent level momentum resolution is desirable. Fast simulations indicate that the position and momentum requirements can be met with a detector with better than $300 \mu\text{m}$ resolution per position measurement in the radial dimension in a multi-plane detector with a span of approximately a meter. Since there is no curvature in the vertical dimension, the resolution requirements are significantly relaxed in that dimension. The long extrapolation from the tracking detector to the muon decay point requires that multiple scattering be minimized and that the material associated with each tracking plane be below 0.5% radiation length.

The trackers are required to reside in vacuum chambers in a vacuum of approximately 10^{-6} Torr and have either a vacuum load on the system below 5×10^{-5} Torr l/s or include a local increase in pumping speed near the tracker.

The tracker must be located as close to the stored muon beam as possible without inter-

fering with the NMR trolley. Any passive material for the tracker should be located outside ± 4 cm from the beam center in the vertical dimension to prevent degradation of the positron energy measurement in the down stream calorimeter. Tracking planes should be as close together as possible to maximize acceptance for low momentum positrons while the first and last planes should be as far apart as possible to provide sufficient lever arm for the long extrapolation of high momentum positrons back to the muon decay point.

Any perturbations to the magnetic field due to material or DC currents must be below 10 ppm at the center of the storage region over an azimuthal extent of greater than 2° . Any perturbations due to transient currents on time scales below 1 ms must be below 0.01 ppm since these cannot be detected or monitored with NMR [3]. The requirements are summarized in Table 19.2.

19.3 Preliminary Design

The preliminary design is an array of straw tubes with alternating planes oriented 7.5° from the vertical direction. We refer to the plane with negative slope as the U plane and the plane with the positive slope as the V plane with respect to the radial-vertical plane. The DC nature of the beam requires a tracker with multiple planes spread out over as long a lever arm as possible. The required number of planes, along with the need to minimize multiple scattering lead to the choice of a gas based detector. The requirement to place the detectors in the vacuum leads to the choice of straws since the circular geometry can hold the differential pressure with minimal wall thickness.

Parameter	value	comments
Impact parameter resolution	1 mm	Set by RMS of the beam
Vertical angular resolution	$\ll 10$ mrad	Set by angular spread in the beam
Momentum resolution	$\ll 1\%$ at 1 GeV	Set by calorimeter resolution
Vacuum load	5×10^{-5} Torr l/s	assumes 10^{-6} Torr vacuum and E821 pumping speed
Instantaneous rate	10 kHz/cm ²	Extrapolated from E821
Ideal coverage	16×20 cm	Front face of calorimeter
Number of stations	≥ 2	Required to constrain beam parameters
Time independent field perturbation	< 10 ppm	Extrapolation from E821
Transient (< 1 ms) field perturbation	< 0.01 ppm	Invisible to NMR

Table 19.2: Summary of the major requirements and environmental considerations for the tracking detectors.

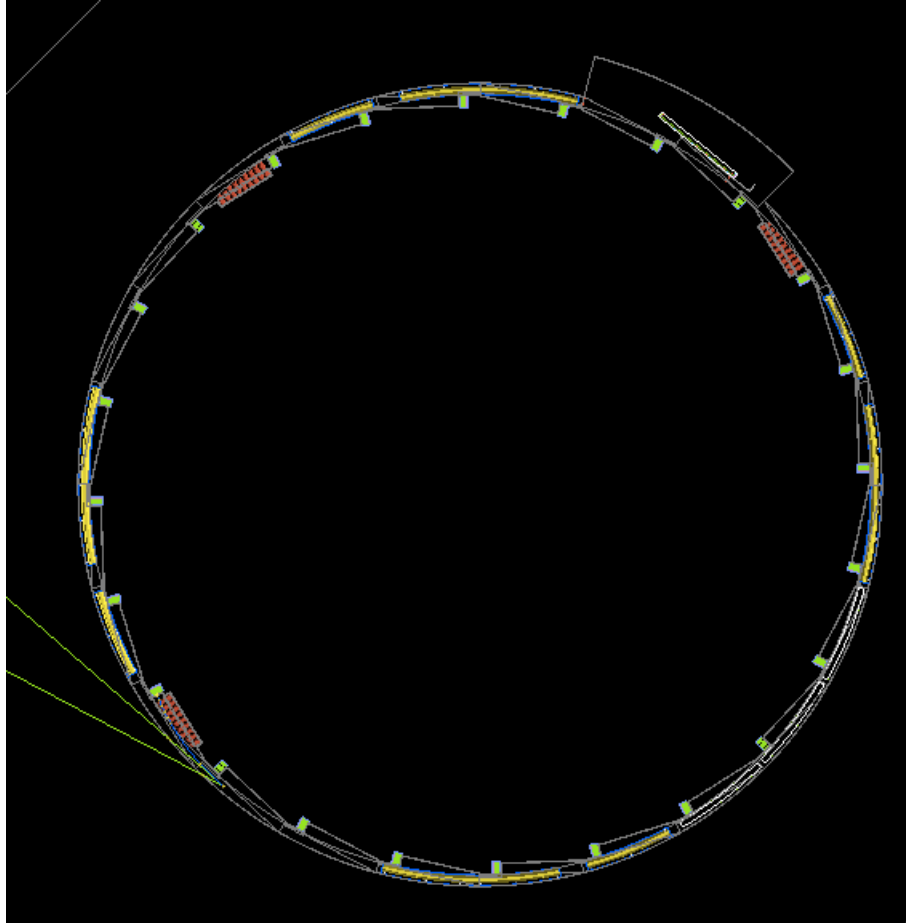


Figure 19.5: Placement of the tracking detectors in the muon storage ring. The detectors can be seen in red in front of calorimeter stations 3, 15, and 21.

19.3.1 Mechanical Design

The design is to have three tracking stations placed at approximately 15, 180, and 270 degrees from the injection point respectively as shown in Fig. 19.5. From these locations they have a clear line of sight to the muon beam unobstructed by quadrupoles or collimators. The vacuum chambers in these locations will be modified to provide radial space for the trackers and to contain flanges that allow for installation and servicing of the tracking detectors (see following sub-section).

Each tracking station consists of 8 tracker modules as shown in Fig. 19.6. The modules

	Straws	Modules	Spares	Total
Tracking Station	128	8	1	1152
Total for 3 stations				3456

Table 19.3: Total number of straws in the tracking system including spares.

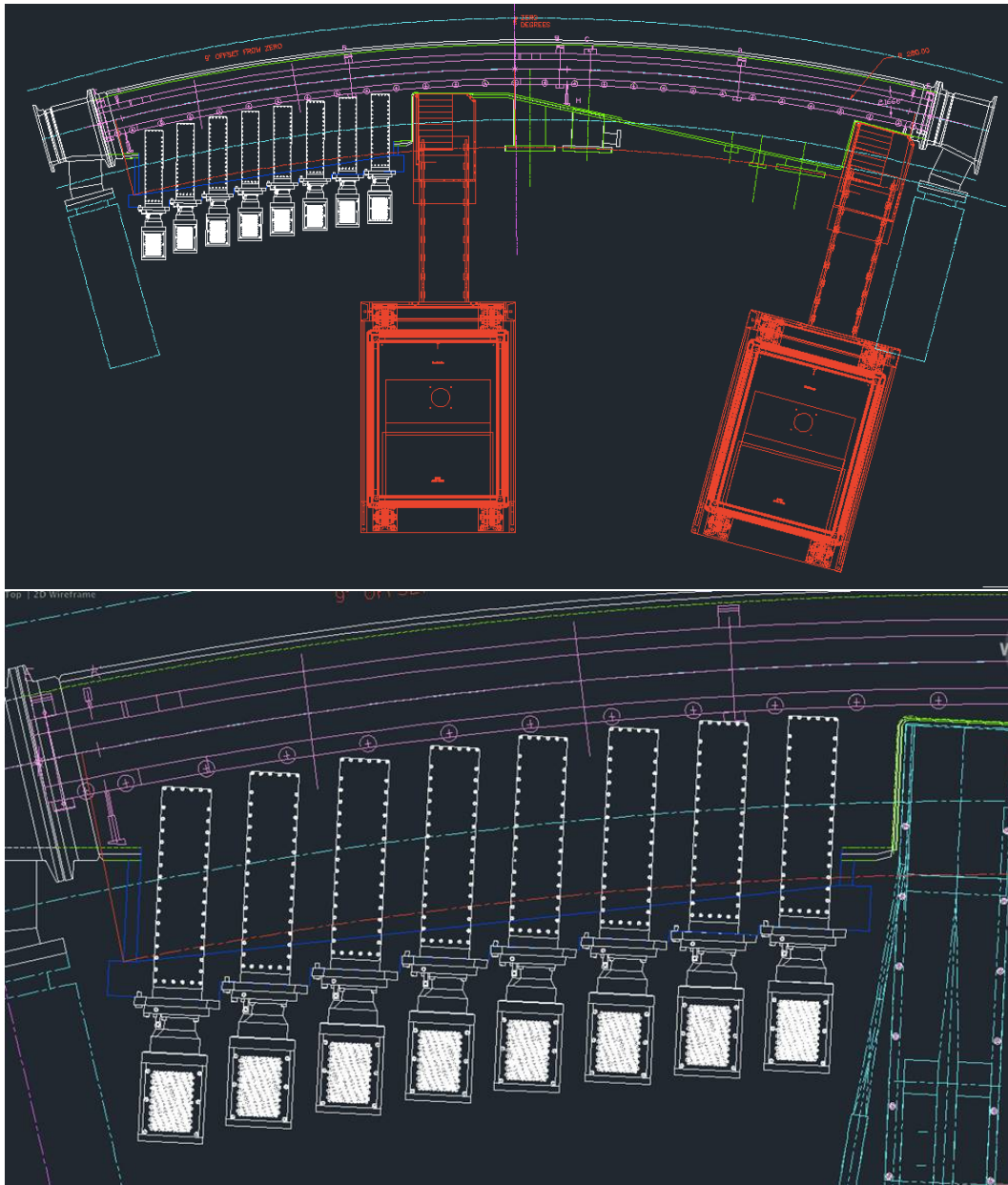


Figure 19.6: Placement of the straw tracking modules in the scallop region of the vacuum chamber. The top figure shows the tracker placement in the upstream section of one of the 12 vacuum chambers and its location with respect to the two calorimeter stations and sleds (red) in the same vacuum chamber. The trolley rail system (purple) is displayed inside the vacuum chamber.

slot into the 'staircase' walls of the modified vacuum chambers. This design maximises radial coverage whilst avoiding the need to manufacture modules with several different lengths. The tracker modules have four layers of straws arranged as two close-packed doublet planes in a UV configuration oriented $\pm 7.5^\circ$ from the vertical direction.

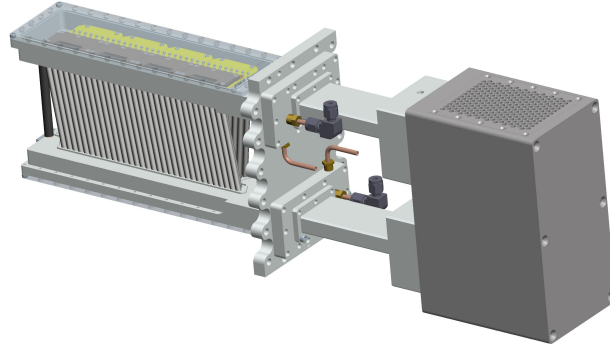


Figure 19.7: Schematic diagram of a tracking module together with the readout electronics attached. The module is 32 straws wide.

Straw material	Aluminized Mylar
Straw wall thickness	15 μm
Wire	25 μm gold-plated tungsten
Straw length	10 cm
Stereo angle	$\pm 7.5^\circ$ from vertical
Gas	50:50 Argon:Ethane
Pressure	1 Atm
Operating voltage	1800 V

Table 19.4: Summary of the properties of the tracking detectors.

Material	Thickness	radiation Length (cm)	X/X_0 (%)
Gold	200 Å	0.3	6×10^{-4}
Aluminum	500+500 Å	8.9	1×10^{-4}
Adhesive	3 μm	17.6	2×10^{-3}
Mylar	6 + 6 μm	38.4	3×10^{-3}
Ar:Ethane	5 cm	1×10^5	4×10^{-2}
Total per straw			0.05
Total per station			0.11
Tungsten	25 μm	0.35	0.7
Total after hitting 1 wire			0.82

Table 19.5: material budget in the active region of a station.

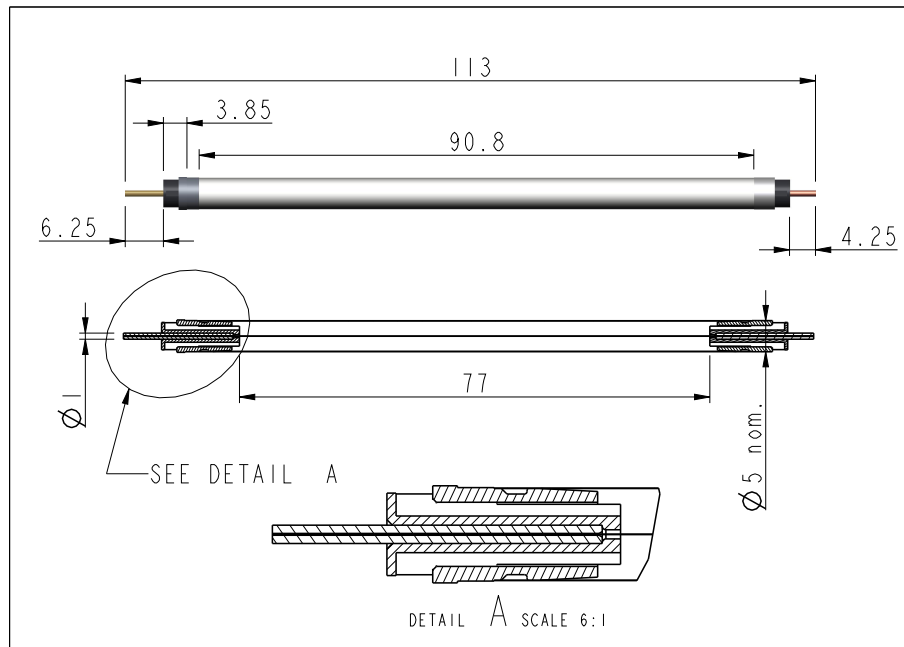


Figure 19.8: Side view and cross-section of assembled straw. The aluminum end-piece on the right is designed to pass through holes in the manifold. The 'top hat' structure of insert on the left will not. Straws are tensioned against this before being epoxied into place. Plastic inserts (shown red) and crimp pins are press-fitted into the aluminum inserts. The pins center the wires and hold them under tension and provide electrical connection to the first-stage electronics.

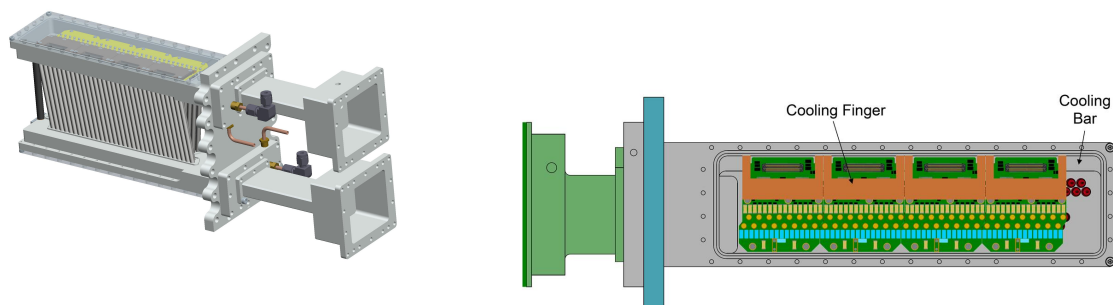


Figure 19.9: Water cooling system for the modules. Heat generating chips are thermally linked connected to a cooling bar machined into the manifold manifold (right). The bar is cooled by water flowing through a longitudinal hole containing a concentric tube for the return flow (left)

The modules are 32 straws wide (i.e. contain 128 channels each). The total channel count including prototypes and spares is listed in Table 19.3.

A schematic diagram of a module is shown in Fig. 19.7. The active height of each station is 7.63 cm. The straws are mounted between aluminum gas manifolds which also house the first stage of the readout electronics.

We have chosen a system based on Mu2e straws [4]. Each straw has a 5 mm diameter and is 10 cm long. The straw wall is made of two layers of 6 μm Mylar, spiral wound, with a 3 μm layer of adhesive between layers. The total thickness of the straw wall is 15 μm . The inner surface has 500 \AA of aluminum overlaid with 200 \AA of gold as the cathode layer. The outer surface has 500 \AA of aluminum to act as additional electrostatic shielding and improves the leak rate. The straws are attached to the manifolds at the ends and tensioned to 65 grams to compensate for expansion under vacuum. The straw parameters are summarized in Table 19.4. The material budget in the active region of each station is given in Table 19.5.

Aluminum endpieces are glued into the straw ends with a combination of silver and structural epoxies. The endpieces locate into holes in the manifold and provide electrical contact for the straws in the aluminum manifolds. The sense wire is 25 μm gold-plated tungsten centered in the straw. The wire is tensioned to 30-50 grams and held in place by a crimp pin embedded in a polycarbonate insulator inserted into the aluminum end-pieces, as shown in Fig. 19.8. The plastic inserts contain slots to allow gas-flow through the straws.

The wire will be held at a voltage of 1800 V. The drift gas is 50:50 Argon:Ethane. This provides gain $\sim 2 \times 10^6$ and radial position resolutions ~ 100 microns.

The top and bottom manifolds of each station extend to the inner wall of the vacuum chamber where they are mounted to a flange. Each manifold is machined from a single piece of aluminum. The pattern of holes for the straws is a compromise between the need to pack the straws as closely as possible to maximize acceptance and the practicalities of machining. Although a prototype with closer packing was successfully machined, the techniques used would be too time consuming for the production trackers. Simulations have verified that the acceptance with slightly wider spaced doublets remains adequate. The box-like structures have aluminum lids with indium seals to close them off. The top and bottom manifolds are bolted to the end-flange again with indium-seals providing the vacuum tightness. This enables the entire station to be inserted into the vacuum as a single piece. The flange contains feed-throughs for the water cooling and is attached to snouts (see Fig. 19.7) which route the electronic signals to the TDC boards. The gas inlet and outlets are also attached to the snouts. This arrangement means that no vacuum feed-throughs are needed. In addition to the support provided by the end flange, the manifolds are held at a fixed separation by carbon fibre posts. This separation must be maintained under forces from tensioning of the straws and sense wires balanced by expansion when the station is in vacuum. A full FEA analysis is needed to determine the distribution of straw and wire tensions in the final design. The eight tracking stations are closely packed in the scalloped region.

Cooling System

The in-manifold electronics, in particular the 8 ASDQ chips generates 4-5 Watts and require cooling. The trackers are water-cooled. The flow of chamber gas helps to maintain a uniform temperature distribution. The interior space of each manifold has a cooling bar in the form

of a 'shelf' machined into one edge. It is drilled longitudinally with a 5mm hole into which a 3mm aluminium tube is inserted. This tube is wrapped with a spiral of wire to keep it concentric with the hole. Chilled water flows in through inner tube and back through the gap between the inner tube and the hole. The ASDQs are thermally connected to the cooled shelf via copper cooling fingers (see Figure Fig. 19.9). Simulations indicate a temperature differential of $\sim 3C$ between input and output water temperature.

Vacuum Chamber Modifications

There are three design considerations that drive the design of the vacuum chamber modifications. First is the desire to use all possible space (14.8 mm) in the interior of the vacuum chamber for the tracking modules. Second is the desire to be able to replace a single module with a spare with minimal down-time in the event that a straw or wire is broken or a problem arises in the readout electronics. Third is the desire to attach the tracking modules directly to a flange to simplify insertion and maintain alignment.

These considerations all lead to the need for the flange bolt pattern to be outside the present vacuum chamber height. For the current vacuum chambers, that is impossible since they are constrained to be between the pole pieces of the main magnet. This requires that the vacuum chambers be extended in the radial dimension so that the flange can be added with sufficient clearance from the pole pieces.

The design of the modified chamber is shown in Fig. 19.10. The extension will be welded onto the existing chamber. The vacuum chamber modifications will be done in the Boston University Scientific Instrument Facility (SIF), where the components of the E821 chambers were fabricated. To minimize the number of welds needed, the extension to the chamber will be fabricated of of a single piece of stock, rather than making it from four or more pieces welded together. This design is at the strong urging of Heitor Mourato, the Director of the SIF, who points out the multiple welds will both deform and soften the aluminum, perhaps compromising the integrity of the chambers.

A further design consideration is the desire to add pumping speed locally near the straws. A vacuum port will be added to the bellows in front of the vacuum chamber. A cryo pump will provide 1200 l/s additional pumping speed for Argon. A secondary vacuum wall made of aluminized mylar will also be placed between the tracking station and the muon storage region. This adds material in front of the tracker so the wall will be designed so that it can easily be removed if it is not required.

Gas Distribution

An 50:50 mixture of Argon:Ethane will be distributed independently to each tracker module with the supply entering the top manifold and the return exiting the bottom manifold. The nominal flow rate is 15cc/min/module. The gas will be stored in a trailer next to the Muon $g - 2$ building and the gas purity will be verified for each gas shipment.

The gas system is shown in Fig. 19.11. The entire system can flow either N₂ or Ar:Et. Flow rate sensors are placed on the supply and return lines for each module. Gas flow to each module is controlled with a solenoid with shut off capabilities controlled by PLC. Input and output bubblers maintain atmospheric pressure in the system. Check valves are in place

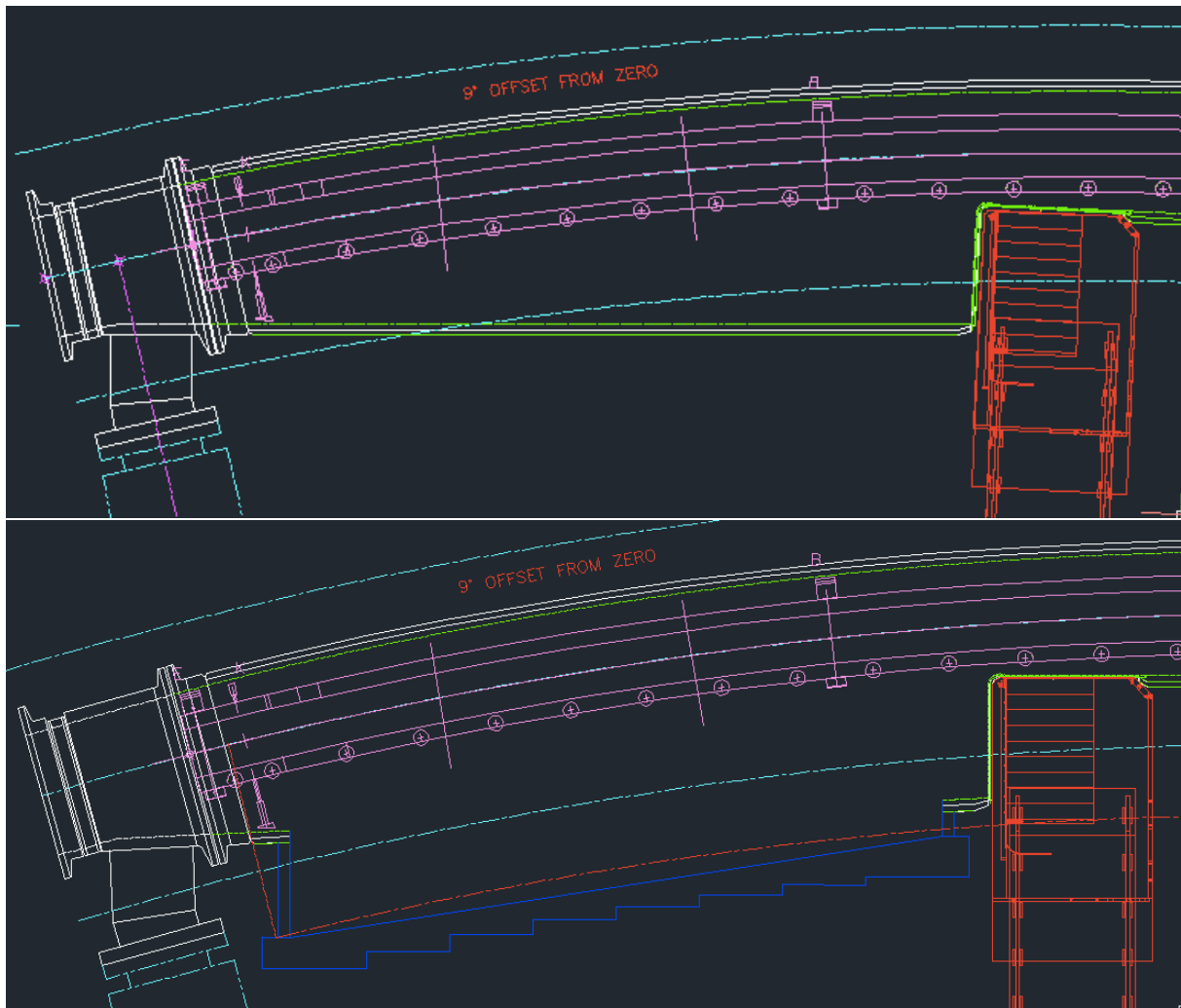


Figure 19.10: Modifications to the vacuum chambers to allow for the tracking stations. The distribution above is an unmodified chamber. The distributions below are a modified chamber. The green lines are the existing vacuum chamber. The blue lines are the extension.

upstream of the output bubbler to prevent oil from being drawn back into the system if gas flow is cut off while the straws are under vacuum. The final return is vented to atmosphere on top of the fenced in berm behind the MC-1 building.

The total charge in the hottest region is expected to be 3 mC/cm. For a pure mixture of 50:50 Ar:Et. we would expect a 20% loss in pulse height over the lifetime of the experiment based on the literature [6]. The aging process can be eliminated with the proper additive. Based on CDF experience, we plan to introduce part per mil concentration levels of O₂ in the gas mixture.

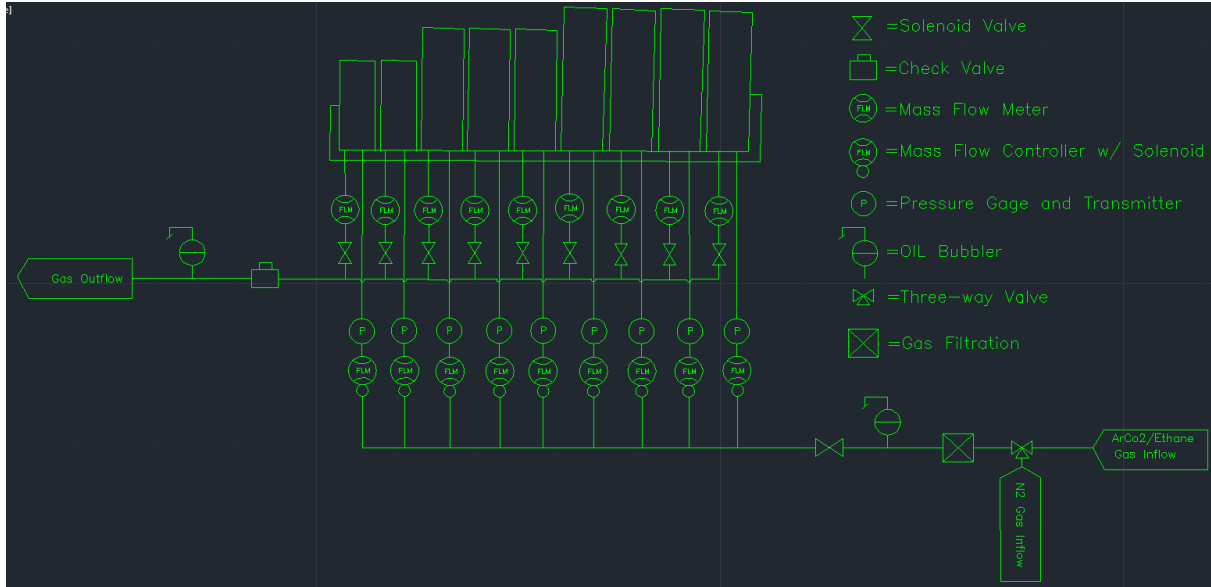


Figure 19.11: Schematic of the gas distribution system

19.3.2 Readout Electronics

Front-End Readout Electronics

The design of the front-end readout electronics is illustrated in Fig. 19.12. Groups of 16 straws are connected directly to an *ASDQ* board containing two 8-channel ASDQ [7] chips. These ASDQ chips process analog signals and send digital signals over Flexicables to a *TDC* motherboard outside of the gas volume. Each TDC motherboard contains two TDCC boards that serve two ASDQ boards, for a total of 64 straw channels per manifold. A *Logic* board, which serves as an interface between the ASDQ and TDC boards and the back end electronics, and a *High Voltage* card which provides high voltage for the straws, also sit outside the gas volume. Details on each of these modules are presented in the following sections. A CAD view of electronics setup is shown in figure Fig. 19.13.

The orientation of the ASDQ boards inside the gas manifold can be seen in Fig. 19.14 - the straws are mounted directly to the boards. High voltage is supplied by an external line to each of the ASDQ boards separately. The ASDQ board filters the high voltage and supplies this potential to each straw through a 100 k Ω current limit resistor. This HV is blocked from the signal channels by 2 kV 470 pF SMT capacitors. The board is grounded to the aluminum manifold via seven aluminum stand-offs to which the board is screwed.

The connection from the straws to the ASDQs is sketched in Fig. 19.15. A protection circuit consisting of four Shottky diodes in a 2x2 mm DFN package provide bipolar protection for both the primary and inverting ASDQ inputs and a 10 Ω series resistor limits peak current.

The role of the ASDQ ASIC [7] is to provide amplification, shaping, a discriminator and charge measurement for eight straws. Though developed for the CDF Central Outer Tracker, it provides a good match to the Muon $g - 2$ tracking detector requirements. It provides fast charge collection (≈ 7 ns), good double pulse resolution (≈ 30 ns), low power

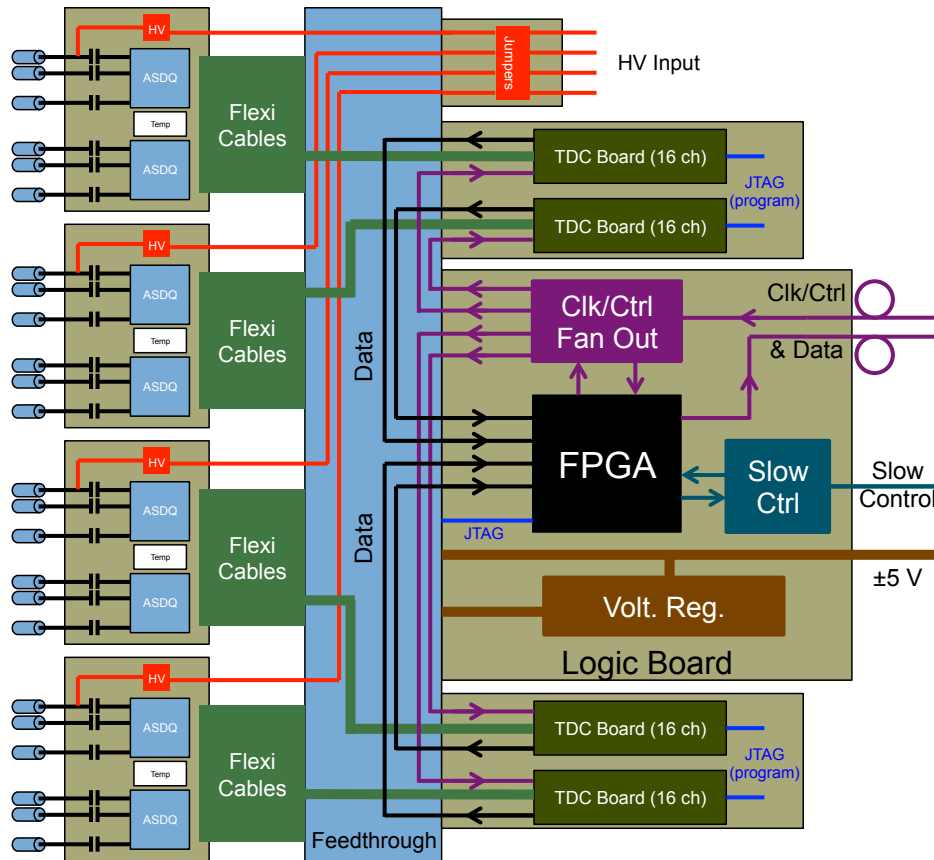


Figure 19.12: Tracker Readout Electronics for 64 straws. 16 straws connect directly to each ASDQ board, which then pass digital signals to a TDC board.

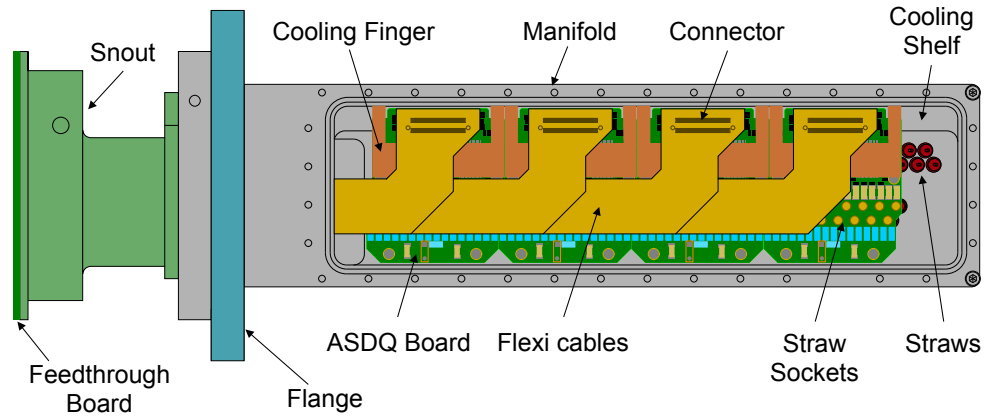
(≈ 40 mW/ch) and low operational threshold (≈ 2 fC). Baseline restoration and ion tail compensation using a pole-zero cancellation technique are provided. The output of each ASDQ is eight LVDS pairs, with leading edge representing the threshold crossing time and the pulse width proportional to input charge.

Several tools for control and calibration of the ASDQ ASICs are available. The thresholds for the leading and trailing edge discrimination can be controlled externally. The width of the discriminator pulse can also be adjusted by varying the drain current into the integrating capacitors of the ASIC's discriminator circuit. The ASDQ ASIC is equipped with calibration circuits which, with an external trigger, can feed realistic input pulses into the front end. Using the calibration circuits, the circuit delay time and pulse width-to-input charge relationship can be determined on a channel by channel basis. The ASDQ boards dissipate approximately 1 watt per manifold. Thermal energy is removed from ASICs by a copper cooling finger, which transfers heat to a water cooling-line.

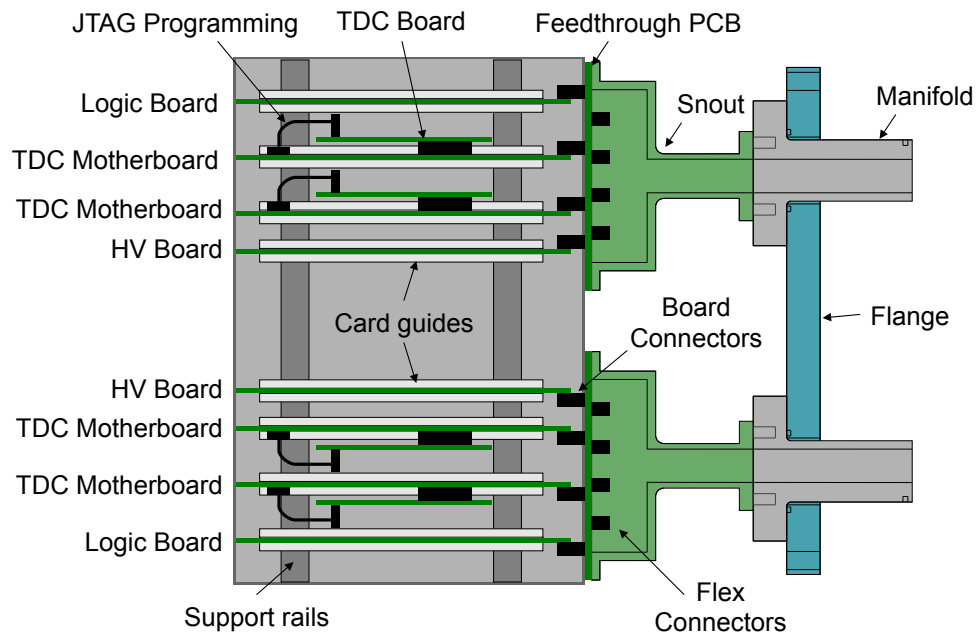
In the previous design, the ASDQ and TDC boards were both located in the gas manifold. Because of cooling problems, the TDC boards have been moved out of the manifold. In this new design, the LVDS pairs produced by the ASDQ are carried through Flexicables to the

TDC boards. There are four Flexicables (of different lengths) per manifold, eight in all per station. The Flexicables have a differential impedance of $100\ \Omega$. The Flexicables also carry power (± 3 volts, $+1.4$ volts), control signals, reference voltages and calibration pulses in to the ASDQs, as well as the output of local temperature sensors. The Flexicables are coupled to the ASDQ boards with 80 pin header connectors and Zero Insertion Force (ZIF) connectors on the output (TDC) side. Because of the relatively long path through the Flexicables to the TDC boards, the LVDS signals from the ASDQ are buffered on the TDC boards before being processed by their FPGAs.

The connection between the Flexicables and the TDC boards is shown in Fig. 19.13(b). The TDC motherboards are mounted outside the gas volume in an electronics rack known as the Flobber (Frontend Low voltage Optical Box to BackEnd Readout). Signals which pass between the detector and the Flobber pass through a snout which is mounted to a flange on the manifold. A *Feedthrough* board, adjacent to the Flobber and mounted on the snout, passes signals in and out of the gas volume, serves as a data bus and also provides a seal for the gas volume. The electronics modules within the Flobber dissipate approximately 11 watts per manifold. To keep the modules from overheating, the Flobbers are each equipped with cooling ductwork connected to remote fans.

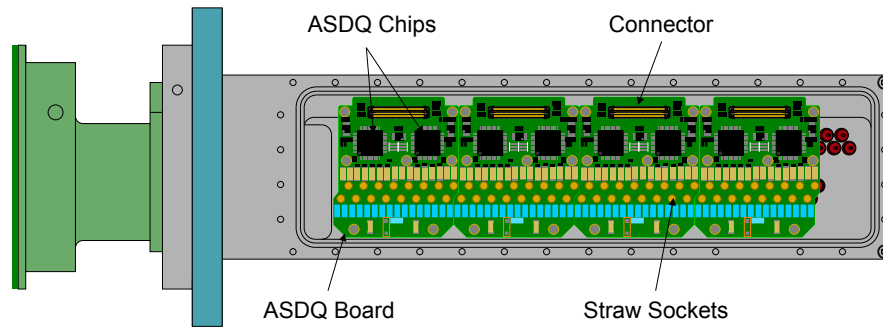


(a) Top View of Manifold Electronics

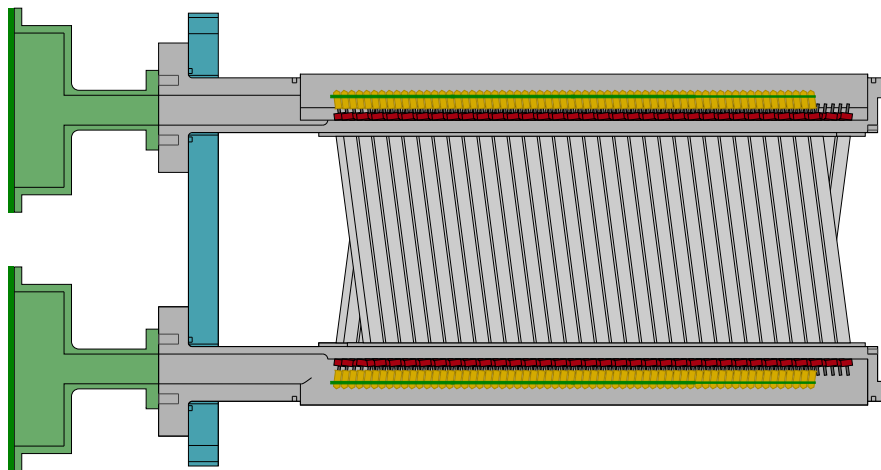


(b) Front View of External Electronics

Figure 19.13: Top down view of electronics and Flexicables within gas volume (Top), side view of external electronics (Bottom).



(a) Top View of Four ASDQs boards in Manifold



(b) Side View of ASDQ boards and straws

Figure 19.14: Top view of electronics within gas volume (Top), side view of internal electronics and straws(Bottom).

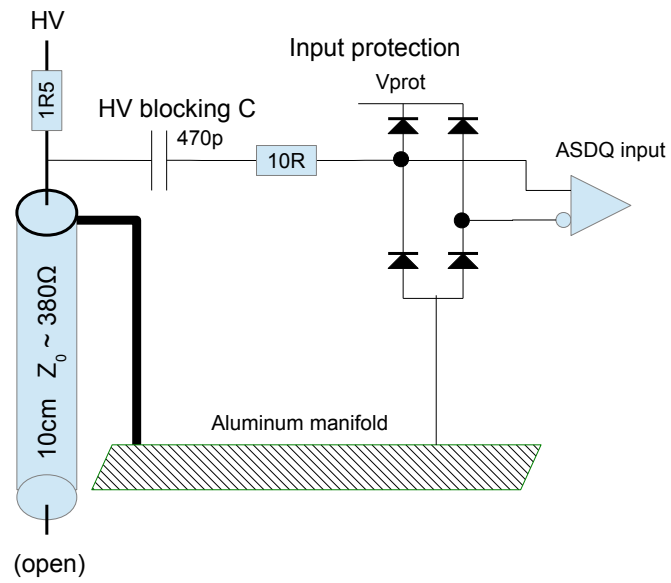


Figure 19.15: Connection between a straw and an ASDQ input.

The TDC modules consist of a TDC motherboard and two daughtercards. Each TDC daughtercard handles two ASDQs (16-channels) and digitizes their output to an accuracy of 625 ps LSB. The TDC circuits are implemented in Altera EP3C5F256C6 FPGAs and the design uses about 50% of the FPGA logic resources. A reference clock of 10 MHz is provided externally on an LVDS signal pair with multiplexed trigger and control signals. The clock is multiplied internally to a four-phase 400 MHz clock for time measurement and internal operation. Up to 2k TDC hits are stored on-chip and read out over a single serial link at 25 MHz. A block diagram of the TDC is shown in Fig. 19.16.

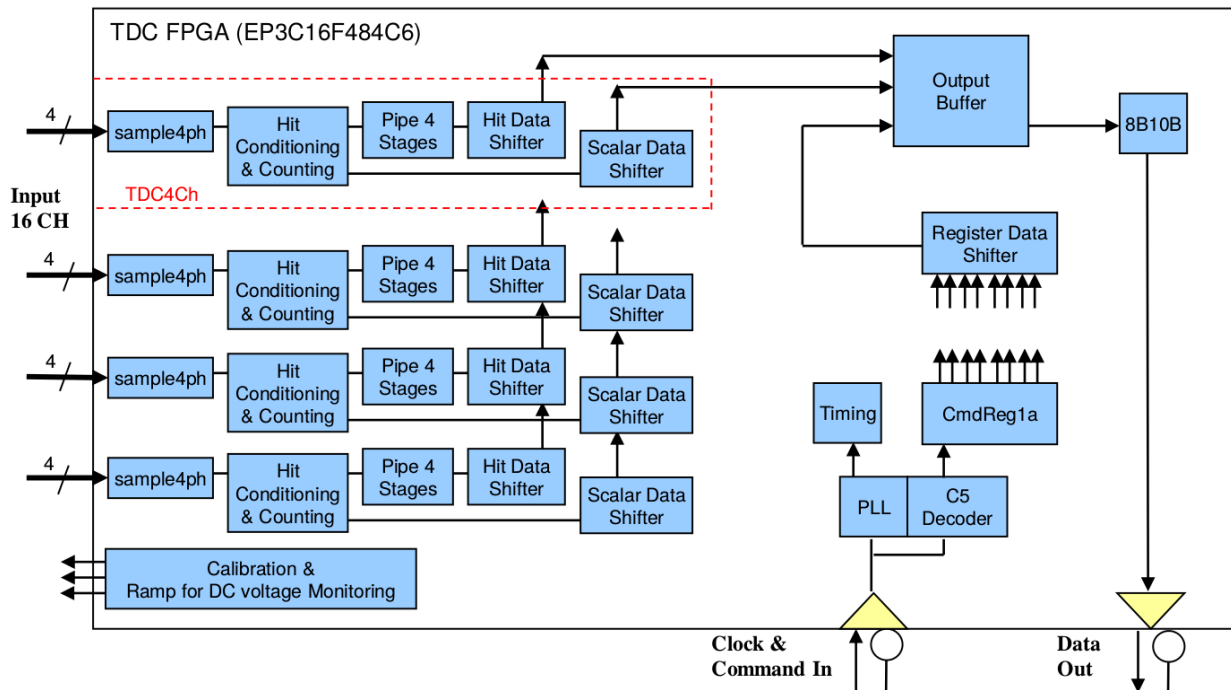


Figure 19.16: TDC Block Diagram

In response to a start-of-spill command, the TDC will commence a capture/readout cycle for one spill. A timing diagram is shown in Fig. 19.17. The start command resets the TDC time stamp to zero and (after a programmable delay) activates the TDC time recording. Up to 2016 hits are recorded during a programmable window, which would typically be 700 μ s to 1 ms. At the end of this window, the TDC can optionally digitize DC voltages or other quantities to be monitored using a Wilkinson ADC scheme with external voltage ramps. At the end of this period the data is transmitted to the Logic Board.

The TDC interface consists of two LVDS pairs carrying serial data. The input clock/command stream is encoded using the C5 (Clock-Command Combined Carrier Coding) protocol at a rate of 10 MHz. The output data is 25 Mbit/sec serial encoded using 8b10b.

The C5 protocol is a DC balanced coding scheme for transmitting messages along with clock in a single channel. Rising edges are equally-spaced at 100 ns and used to recover a 10 MHz clock. Three pulse widths (25%, 50% and 75% of the bit period) are used to encode commands. An idle pattern of 50% pulses is sent when no commands are being transmitted.

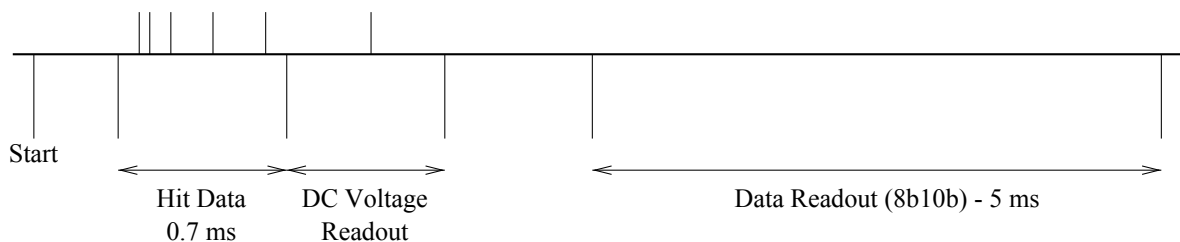


Figure 19.17: TDC Timing Cycle

Various specific patterns are used to trigger actions in the TDC. The C5 data and control codes are shown in Table 19.6 along with the use defined for $g-2$. Several registers control aspects of the TDC operation, as listed in Figure 19.18.

4B/5C Codes	Widths of Pulses					$g-2$ Meaning
	0	1	2	3	4	
Q0	0	0	0	0	0	Idle
D15	+1	-1	+1	-1	0	Reset Spill Number
D14	+1	-1	+1	0	-1	Reset Time
D13	+1	-1	0	+1	-1	Set Next Spill Type n
D12	+1	-1	0	0	0	Start of Spill

Table 19.6: C5 Codes for TDC Control. “+1” means wide pulse, “-1” means narrow pulse and “0” means nominal (50%) pulse.

The TDC transmits data using 8b10b coding, a common DC-balanced scheme used in popular networking standards such as Gigabit Ethernet. A detailed description of the coding is beyond the scope of this document, but it is similar in spirit to the C5 scheme. Each 8 bit byte is encoded using a sequence of 10 bits. Codes are chosen to optimize DC balance and to limit the length of runs of successive ‘0’ or ‘1’ values. In addition to the 256 data codes, several control codes are used. A common representation for the symbols is D.x.y for data codes, where x is the decimal representation of the first 5 bits and y is the decimal representation of the final 3 bits. The control codes are represented as K.x.y where x and y are defined as for data. Many codes have two encodings with differing numbers of ‘1’ and ‘0’ bits, which are selected by the encoder logic to maintain DC balance.

When idle, the TDC continuously sends the K.28.5 code, which is a special control code containing a so-called “comma sequence” of binary “0011111” or “1100000” which cannot be found in any bit position in normal codes. This is used by the receiving logic to acquire bit synchronization. After receiving a start command and acquiring hit data, it sends the special K.28.1 code followed by up to 2048 32-bit words, formatted in a data record as shown in Fig. 19.19.

A Logic board is connected to the Feedthrough board and mounted in the Flobber. The Logic board collects data buffers from the TDCs, in 8b10b format, buffers, labels and

addr	15	14	13	12	11	10	9	8	7	6	5	4	3	2	1	0	notes	
0	0											$clk_{C5,TDC}$	$Idle_{sw}$	En	reset			
1	0						Scaler	Edges	SW	Addr	HW	Addr						
2	Channel enable mask																	
3	TDC start time																	
4	TDC selb time																	greater than start
5	TDC end time																	greater than selb
6	TDC readout time																	greater than end
7	Reg 7																	unused
8	Reg 8																	unused
9	Reg 9																	unused
10	Reg 10																	unused
11	Reg 11																	unused
12	Reg 12																	unused
13	spill time 15:0																	
14	spill number 15:0																	
15	Reg 15						DeMultiPW											

Figure 19.18: TDC register map

assembles them, then transmits the data packets to the backend electronics. The Logic board has room to buffer up to five spills from each TDC. The data format is outlined in Fig. 19.20. The Logic board reads TDC data from the TDC cards in parallel at 4×25 Mb/s and writes it out at 125 Mb/s, in 8b10b format. The Logic board keeps track of the event type and number and compares those values with those of the TDC buffers that it reads out. The logic board notes discrepancies but does not eliminate data.

The Logic Board controls the clock signals used by the TDCs. In normal data-taking, the clock signal for the TDCs is derived from the input C5 data stream. When the backend electronics' C5-clock lands on the Logic board, it is first run through a 1-to-2 fanout IC. The first copy of the C5-clock goes to the Logic board for use in clocking and receiving C5 commands. The second copy goes to a 2-to-4 fan-in/fan-out IC that generates a copy for each of the four TDCs. The fan-in option of the IC allows for the Logic board to generate its own C5-clock signal, from either the external clock or the on-board oscillator, and fan that out to the TDCs instead. The control over which input should be fanned out is set on the Logic board via the slow control link. **Need chapter reference for slow control here.**

The Logic board has a mezzanine card with low voltage regulators for the ASDQs. The Logic board houses temperature sensors, as well as voltage and current sensors for the ASDQ supplies. If the current monitor senses a current in excess of a safe threshold, it directs the logic board to turn off the regulator. The monitor must then be reset through the slow control system, after which the voltage regulator can be activated again. In addition to power, the Logic board provides external control of the ASDQ ASIC. External voltage references are supplied by the Logic board. Op-amp buffers on the ASDQ board rescale and offset these voltages for use on the ASIC. The Flexicables carry an LVDS pair to trigger the injection of test pulses into the ASIC.

The FPGA on the Logic board reads in control/configuration data from the slow control and passes on that information, with the help of a universal asynchronous receiver/transmitter (UART), to the TDC board. The FPGA can also be used to upload firmware to the TDC

addr	31	30	29	28	27	26	25	24	23	22	21	20	19	18	17	16	15	14	13	12	11	10	9	8	7	6	5	4	3	2	1	0
0	0												0x3C = K28.1																			
1	0												0x67 = 'g'																			
2	0												0x2D = '.'																			
3	0												0x32 = '2'																			
4	0												0x54 = 'T'																			
5	0												0x44 = 'D'																			
6	0												0x43 = 'C'																			
7	Version date: 0x201YMMDD																															
8	size																Channel Mask															
9	0																Spill # [23..0]															
10	Time MSB [43..12]																															
11	0																Time LSB [11..0]															
12	Start time (160ns LSB)																End time (160ns LSB)															
13	SelB time (160ns LSB)																Readout time (160ns LSB)															
14	0																															
15	1-scalars; 0-both edges; others: 0																															
16	Scalar Count 15																															
17	Scalar Count 14																															
18	⋮																															
19	Scalar Count 1																															
20	Scalar Count 0																															
21	0	0	1	edge	Ch: 0-15												Coarse time: LSB 5ns, range 0 - 10.485775 ms												Fine			
-	⋮																															
size-1	0	0	1	edge	Ch: 0-15												Coarse time: LSB 5ns, range 0 - 10.485775 ms												Fine			

Figure 19.19: TDC Detailed Data Format

daughterboards, using a JTAG connection. Although setup and configuration will be handled automatically during actual data-taking, a command line interface is also available for independent test runs.

Two High Voltage boards are also mounted in the Flobber. Each of the High Voltage boards takes four SHV inputs. Each HV line has a bypass capacitor for reducing noise, a current limiting resistor and a jumper for isolating groups of 16 straws, in case of a short. After the current limiting and filtering, the input HV lines are carried to the eight ASDQ boards on separate cables. A return path is also provided.

-	31	30	29	28	27	26	25	24	23	22	21	20	19	18	17	16	15	14	13	12	11	10	9	8	7	6	5	4	3	2	1	0
0	0x3C = K28.1										0																					
1	0										size																					
2	0										Spill # [23..0]																					
3	Time MSB [43..12]																															
4	0										type	FE	Er	OOS	TDC_{EN}	Time LSB [11..0]																
5	TDC0: 31:enabled, 30:OOS, 29: size error										0	size																				
6	TDC1: 31:enabled, 30:OOS, 29: size error										0	size																				
7	TDC2: 31:enabled, 30:OOS, 29: size error										0	size																				
8	TDC3: 31:enabled, 30:OOS, 29: size error										0	size																				
9	0 (TDC: 1)										0x3C																					
-	0										0x67 = 'g'																					
-	0										0x2D = '2'																					
-	0										0x32 = '2'																					
-	⋮																															
-	0 (TDC: 2)										0x3C																					
-	0										0x67 = 'g'																					
-	0										0x2D = '2'																					
-	0										0x32 = '2'																					
-	⋮																															
-	0 (TDC: 3)										0x3C																					
-	0										0x67 = 'g'																					
-	0										0x2D = '2'																					
-	0										0x32 = '2'																					
-	⋮																															
-	0 (TDC: 4)										0x3C																					
-	0										0x67 = 'g'																					
-	0										0x2D = '2'																					
-	0										0x32 = '2'																					
-	⋮																															
size - 3	size																															
size - 2	CRC																															
size - 1	0										0x5C = K28.2																					

Figure 19.20: Logic Board Data Format

Back-End Readout Electronics

FC7 MicroTCA advanced mezzanine cards developed by CMS will provide the clock and control signals for the logic boards and transfer the hit data from the logic board buffers to the DAQ via a CMS AMC13 card [8]. The FC7 has a Xilinx Kintex-7 FPGA, can accommodate two FMCs and has a connection to the AMC13 via the MicroTCA backplane. A photograph of the board is shown in Fig. 19.21.

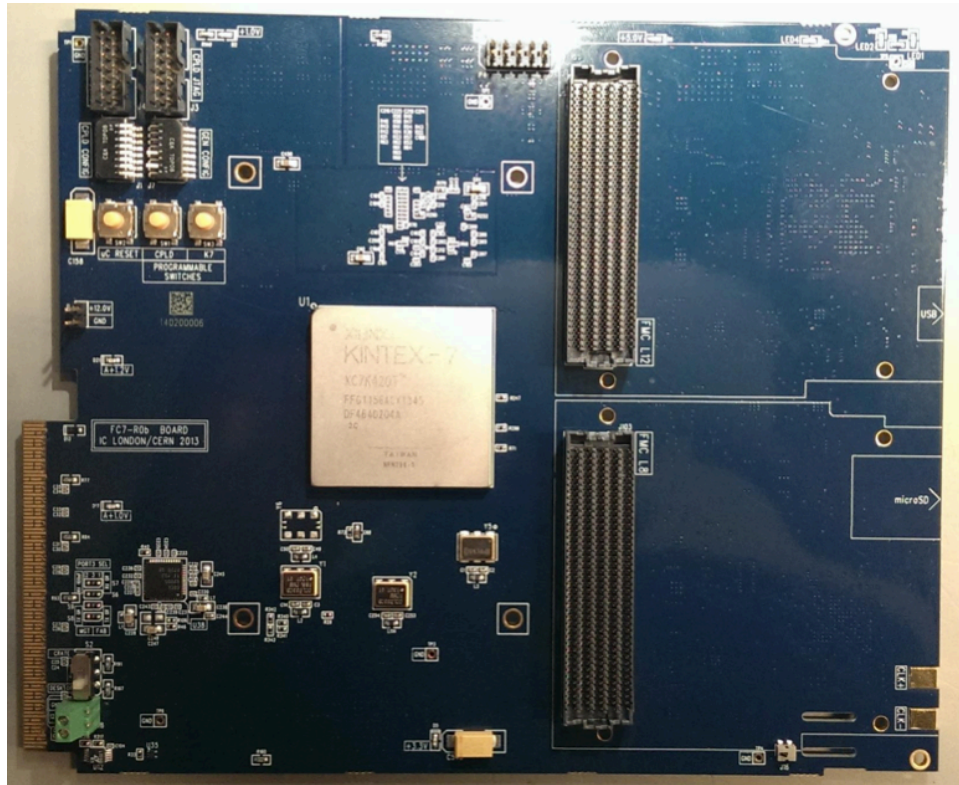


Figure 19.21: A photograph of a prototype FC7. The two FMC connectors are to the right of the Kintex-7 FPGA and allow up to 16 fiber connectors to the front of the board. The backplane connection to the AMC-13/MCH is at the bottom left of the photograph.

It incorporates an MMC providing the IPMI functionality and Gb ethernet via the crate's MCH. The ethernet communication will utilize the IPBus communication tools [9] developed by CMS. The ethernet/MCH interface will be used to upload configuration data and also to send a subset of the data to a local PC to quickly identify issues with data integrity. The FC7 has 30 Mbytes of block ram which is more than an order of magnitude larger than the data volume expected from a single tracker in a single spill. The clock, control and readout data will be transmitted between the FC7s and the logic boards using fiber optic cables. This has the benefit of decoupling the clock/control/data-readout signals from the LV. Potentially this allows the readout crate to be housed in the MC1 counting room away from the storage ring thereby removing the overhead of ensuring that the crate and backend electronics do not perturb the storage ring's magnetic field. One FC7 will be sufficient to readout a single tracker since each logic board will communicate with the FC7 with a single fiber pair (via an

SFP) and each of the two FMCs on the FC7 can accommodate 8 fiber pairs. The data from all three trackers can thus be sent to a single MicroTCA crate which has sufficient slots for 12 AMC cards in addition to the AMC13 and MCH. This allows one spare FC7 per tracker in the crate which will enable a quick recovery, with a simple slot re-configuration, should an FC7 fail. The FMCs housing the 16 SFPs and interfacing the optical signals with the FC7 will be the EDA-02707 that is being used for CMS's new Trigger, Control & Distribution System (TCDS) [10]. A schematic of the MicroTCA readout crate is shown in Fig. 19.22.

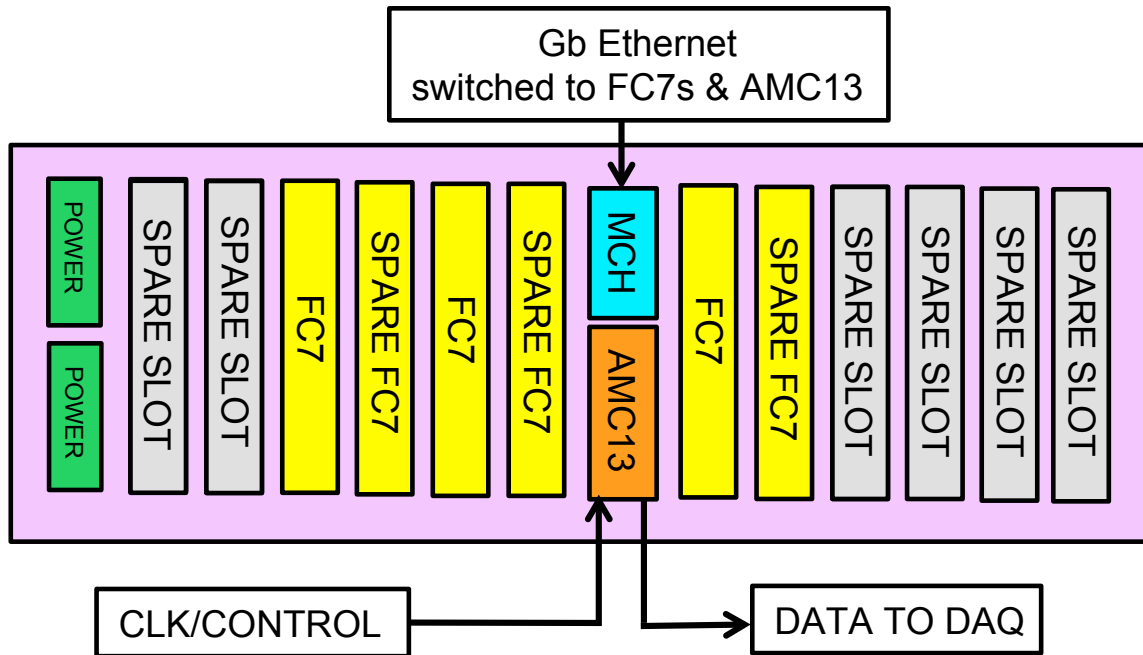


Figure 19.22: A schematic of the MicroTCA tracker readout crate.

The FC7s will receive their clock and control signals from the AMC13 and these will be encoded into the C5 protocol on the FC7 FPGA before being transmitted to the logic boards. The FC7 will receive data in the 8B10B protocol from the logic boards and this will be formatted in the FC7 FPGA to match the data format requirements of the AMC13. The TDCs will begin to accumulate data at a fixed time ($O(30) \mu s$) after the begin of spill signal is received by the AMC13 for a duration of $700 \mu s$. In order to ensure that the tracker hit times have a common t_0 with respect to the calorimeter, sufficient to synchronize the data before track-fitting, the FC7 will multiply the input 40 MHz clock to 800 MHz and will record when the C5 command instructing the TDC to accumulate hits is sent to the logic board with respect to this clock. The C5 commands are sent with a 10 MHz clock and so don't have the necessary granularity to synchronize the data.

A block diagram showing the key features and signal paths of the FC7 is shown in Fig. 19.23.

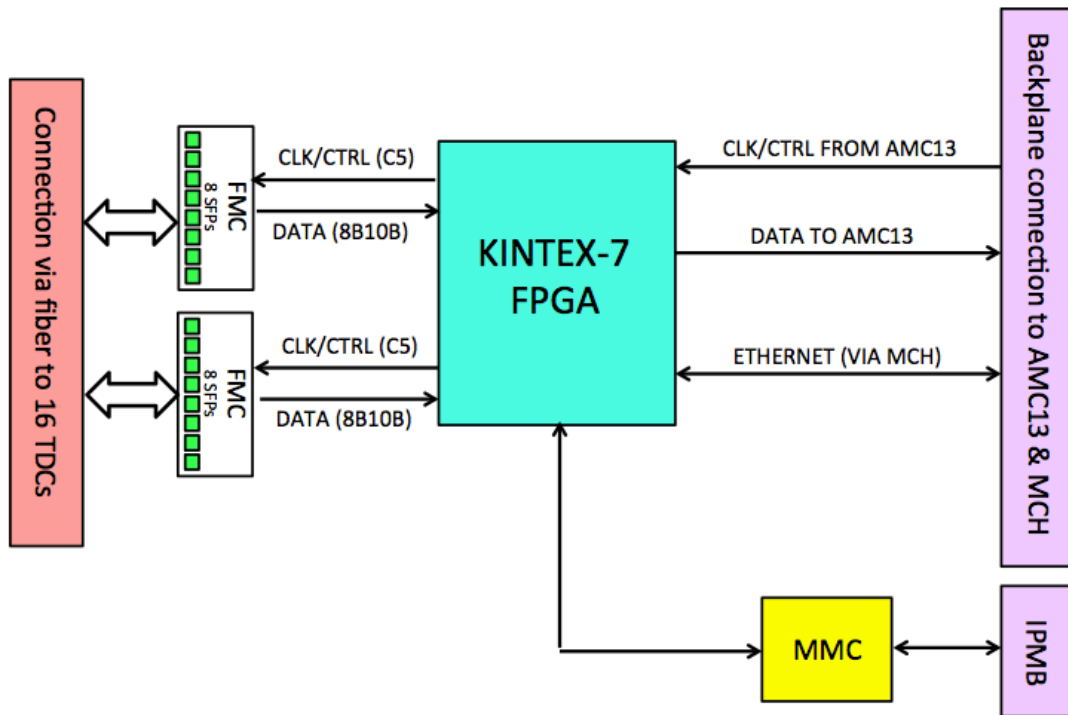


Figure 19.23: A block diagram of the key features and signal paths of the FC7 tracker readout module.

Low-Voltage Distribution

The low-voltage (LV) system provides $\pm 5V$ to the logic board which will be put through regulators to provide the necessary power to the TDCs and ASDQs. The typical operational current is about 2.8A for the +5V supply and 1.4A for the -5V supply. The LV system will provide independent LV to each logic board such that individual logic boards can be powered on and off. The LV boards provide isolated output to avoid ground off-sets between systems which can be a main issue when using long cables.

The LV will be provided by 36W isolated DC-DC converters operating with a 24V DC input supplied by an external commercial AC-DC power supply. The expected power consumption is about 20W so the 36W is chosen to allow for some contingency. One board provides a dual $\pm 5V$ output sufficient to power a single logic board, so 16 boards are required per tracker. A photograph of the board is shown in Fig. 19.24.

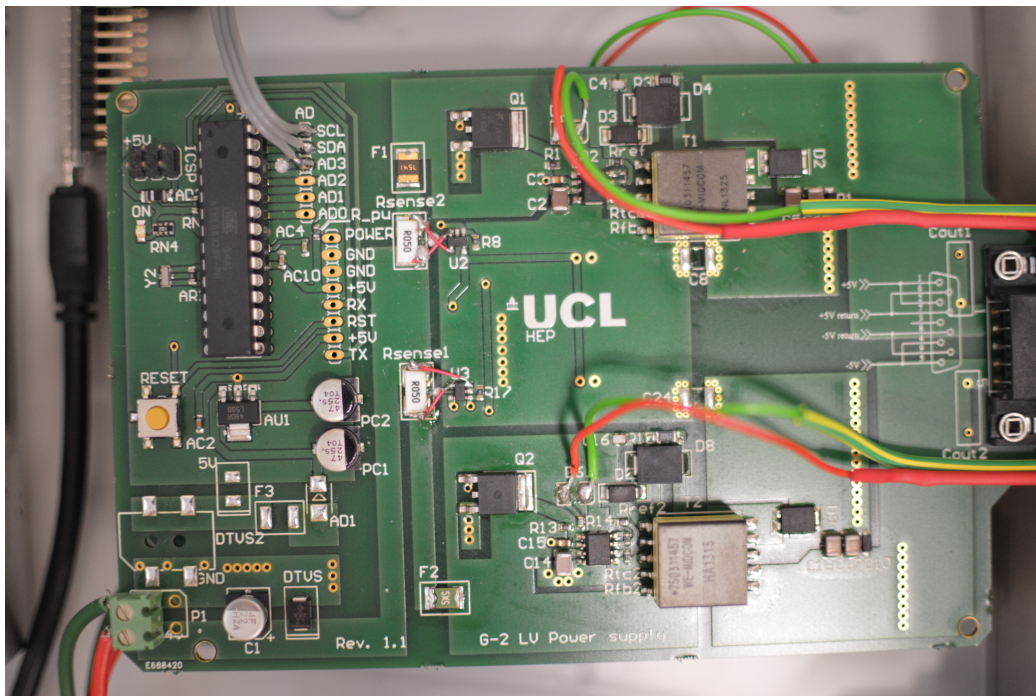


Figure 19.24: A photograph of a prototype low-voltage board.

The boards for one tracker will be housed in a custom 3U crate with a crate controller board which can power individual boards on and off as well as provide monitoring information such as currents and temperatures. The three LV crates will be located in the centre of the ring at a maximum distance of 5m from the logic board so as to minimize signal perturbation and impact on the storage ring field. Furthermore, the LV boards also offer slow control capabilities via direct links to every logic board.

High-Voltage Distribution

High voltage will be supplied by a commercial CAEN SY4527LC universal multichannel power supply system containing 12 channel A1535 3.5 kV/3 mA common floating return boards. The nominal HV will be 1800 V. All electronics in the HV chain are rated to 3kV. Two SY4527s will be located in the center of the ring and will distribute HV to the three tracking stations. There is one common HV per 16 straws so each tracking station has 64 HV channels. Trip currents will be set at 10 μA per HV channel to avoid damaging straw walls if a sense wire breaks.

19.3.3 Monitoring and Slow Controls

The details of the experiment-wide Slow Controls system can be found in Chapter 22. The key parts of this system relevant to the straw tracker system are described below. Details of the slow controls data acquisition, storage, and access are not repeated here.

The Slow Controls system will be used to monitor a variety of parameters in the tracking system, as shown in Table 22.1. Voltages and currents for both the LV and HV systems will be monitored using dedicated functionality built into the standard commercial power supplies and interfaced to the experimental slow control system. Ambient pressure, temperature, and humidity measurements (in the regions near the tracking stations) will be monitored using dedicated sensors. These sensors, and their interface to the slow controls system will be identical throughout the experiment and are described in Chapter 22.

A few parameters monitored by the slow controls system will be unique to the tracking system. Since the straw tracker is a gas-based system, both the gas flow and the gas temperature will be monitored. These sensors will be integrated into the straw tracker gas system, as described in a previous section. The liquid water cooling system will also require the monitoring of several parameters. The flow and temperature of liquid cooling water will be monitored by the slow controls system at several points in the system. Inside the manifold, several parameters will also be monitored. The temperature of the circuit board will be monitored with a dedicated temperature sensor built into the circuit board. The slow controls interface built into the front-end electronics is described in a previous section. This slow controls interface will be connected via a USB interface to a computer in the experimental hall. This computer will be running a MIDAS front-end that will allow this monitored data to be added into the data acquisition system.

The tracking system is critically dependent on both the gas flow and the flow of cooling water. If either of these two systems are compromised, it could result in damage to the components of the system. For this reason, a dedicated interlock system is being constructed (see Sec. 22.2.4). This interlock system will be part of the experiment's main Siemens PLC which is used to ensure the safety of the cryogenic and vacuum systems. It will receive inputs from the flow sensors in the gas and cooling water systems, from the temperature sensors inside the tracker manifolds, and from pressure sensors near the tracker stations. While the logic has not been finalized, the information from these inputs will be used by the PLC to send signals to the LV and HV power supplies in the tracker system to ramp down or turn off the power. The tracker gas system also includes solenoid valves that can be used to quickly turn off gas flow. These signals will also be propagated to the central slow controls system

to ensure that data quality can be adequately monitored. Although the exact logic has not yet been finalized, since the interlock system is based around a PLC, enough flexibility is present in the system to meet our needs.

19.4 Performance

The straw leak rate has been measured to be 3.5×10^{-6} cc/min/per straw for CO₂. This corresponds to a vacuum load per tracker station of 7.7×10^{-5} Tl/s. Given the additional pumping speed, we expect to be able to maintain a vacuum of 1×10^{-7} an order of magnitude below our specification. Furthermore, the permeation of ethane is expected to be significantly lower than CO₂. For example, the measured permeation of Methane through Mylar is 40 times less than CO₂ providing further head room. A measurement with Ethane is underway.

The expected performance of the tracker technical design is determined by a simulation. The simulation is benchmarked by the performance of a 32 channel prototype module that was tested extensively using a ⁵⁵Fe source in the lab and in two beam tests at the Fermilab Test Beam Facility as discussed below. The performance of a single straw is determined using GARFIELD [11]. This program simulates the propagation of electrons and ions in a gas in the presence of electric and magnetic fields based on the measured ion mobility in Argon. Key parameters such as the effective threshold to apply in the simulation are determined using the signal to noise achieved in the prototype and determined in beam. The geometry of the system is determined using a full GEANT4 [12] model of the muon storage ring that includes the proper physics model to simulate muon storage, precession, and decay. The performance of the tracker is determined using a fast tracking software package that takes the positron hit positions from the GEANT4 simulation, applies resolution from GARFIELD and multiple scattering corrections, determines the positron trajectory, and extrapolates back to the point of tangency to determine the muon decay position. The fast simulation currently assumes a uniform magnetic field which is valid for the majority of the tracking volume. A first version of a full tracking code algorithm that uses the GEANT4 hits for input and includes all physics processes for energy loss, multiple scattering, and backgrounds also exists.

The distance versus time ($x - t$) relation determined from GARFIELD are shown in Fig. 19.25 for the case of zero magnetic field and the 1.5 T nominal magnetic field. The resolution as a function of gain and the resolution as a function of closest approach to the wire at the nominal gain are shown in Fig. 19.26. At a gain of 2×10^6 , the straws are fully efficient for single ionizations assuming the noise levels achieved in the prototype electronics. The average resolution is found to be approximately 100 μm providing sufficient headroom to the 300 μm .

The rate in the hottest straw at injection is 200 kHz. At a gain of 2×10^6 , we expect a gain sag of 5% at this rate. Simulations indicate that no noticeable effect is seen since we are fully efficient for single ionizations.

The acceptance to reconstruct at least 5 hits as a function of momentum and as a function of the muon decay distance is shown in Fig. 19.27. There is sufficient coverage at all positron momenta for determination of the muon beam parameters. The loss of acceptance at lower momenta is due to the fact that the lowest momentum positrons originate very close to the calorimeter and the limited available space between the muon decay position and the

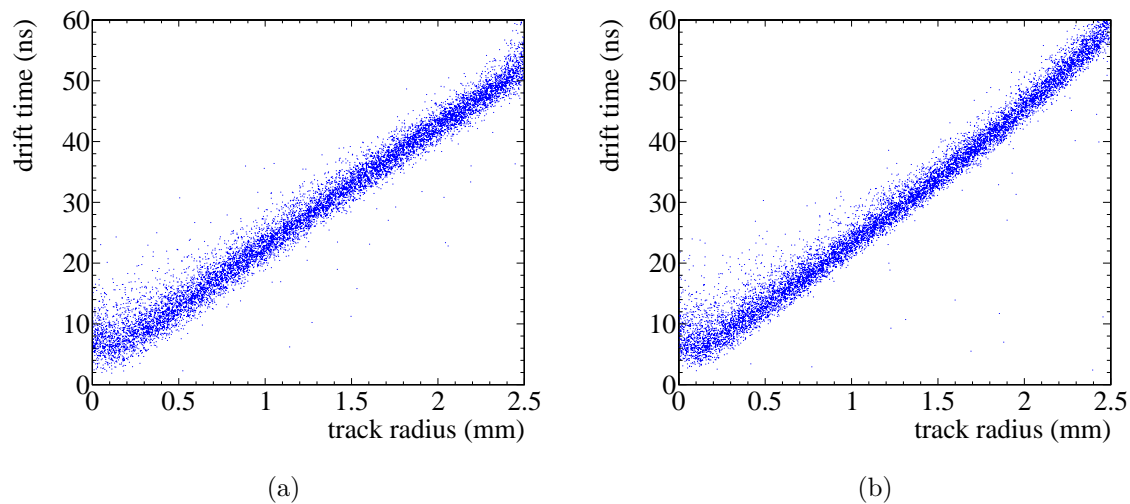


Figure 19.25: Time versus distance relation in a single straw predicted by GARFIELD for 50:50 Argon:Ethane at a gain of $2e6$. The distribution on the left is for zero magnetic field. The distribution on the right is for the full 1.5T magnetic field.

calorimeter limit the amount of tracker planes the positron can hit. The distance between stations is dominated by the area necessary for the readout PCBs. The azimuthal acceptance of the tracker is shown in Fig. 19.28 indicating we can reconstruct the decay positions of muons up to meters upstream of the tracker. The hit density in the tracker is also displayed in the plot.

The momentum resolution, muon decay position, and positron vertical angle resolution for an Ar:CO₂ mixture are shown in Fig. 19.29. At 1.5 GeV, the resolutions are 1 mm on the radial position, 1.5 mm on the vertical position, 0.5% on the curvature, and 1 mrad on the vertical angle. The resolutions on position and momentum rise steeply with momentum but in all cases are below the required values. Both position resolutions become significantly worse above 2.6 GeV. In this region, the muons are decaying between 5 and 10 meters from the first tracking plane and the large lever arm makes a more precise determination impractical. The momentum resolution is worse than for a typical gas based system but is well below the resolution of the calorimeter which satisfies the requirements. The vertical angle resolution is also well below the requirements. The performance is near the specifications for Ar:CO₂ and have significant headroom with Ar:Et.

Two large multi-channel prototypes have been constructed. A 32 channel prototype was constructed based on the conceptual design and is shown in Fig. 19.30. The prototype consists of 2 close packed doublet layers, 8 straws wide in U and V configurations. Prototype ADSQ and TDC boards were housed in the gas return manifolds for each view as shown in Fig. 19.31. All components of the prototype were constructed and assembled in Fall and Winter 2013. The prototype was tested using 120 GeV protons at the Fermilab Test Beam Facility for two weeks in January 2014 and April 2014. The January run was conducted with the straws in atmosphere, the April run was conducted with the straws and manifolds entirely contained in a vacuum chamber.

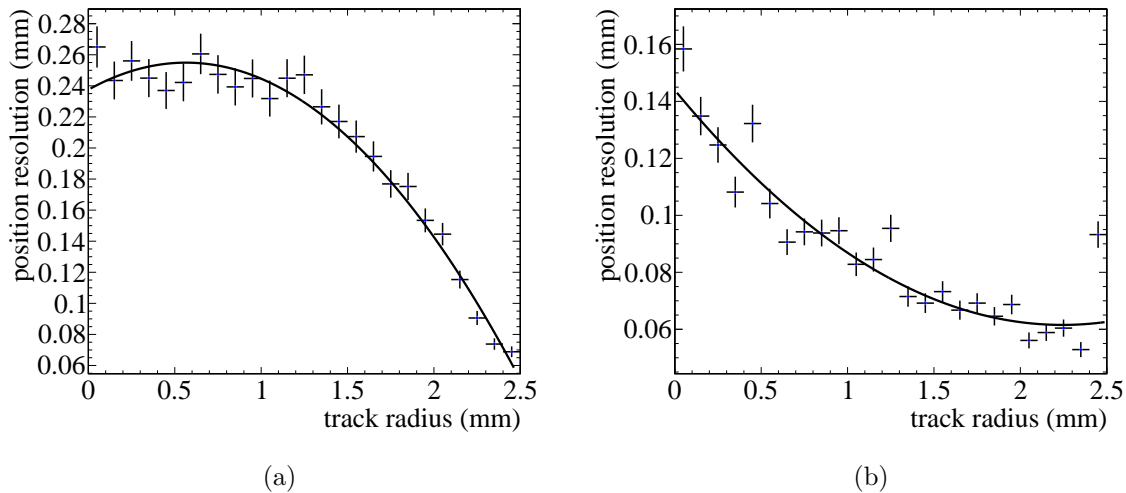


Figure 19.26: (a): The position resolution determined from GARFIELD for a single straw using the derived $x-t$ relation. The distribution on the left is for 80:20 Ar:CO₂ achieved in test beam. The distribution on the right is what is expected for 50:50 Ar:Et. The specification is 300 microns.

A 128 channel prototype based on the full preliminary design was constructed in Winter and Spring 2015 and was tested in beam in June 2015 using Ar:CO₂, Ar:Et, at atmosphere, and at vacuum. The prototype is shown in Fig. 19.32. Results of the beam test are pending.

The hit count in the prototype is shown for one run in Fig. 19.33. The beam is clearly seen in both the U and V layers. Figure 19.33 also shows the time correlation between hits in the doublet layer. Figure 19.34 compares the time difference between hits in a straw doublet between the prototype and GARFIELD. The agreement in the width of the distributions indicates proper modeling of the drift velocity of the gas. Figure 19.35 shows the anti-correlation in drift times between the straws in a doublet. For the data distribution, the drift times in the V view are shown and the T_0 is taken as the average time of the two straws in the U view. The residuals of the correlation are in good agreement indicating proper modeling of the resolutions in GARFIELD once the appropriate threshold is applied to the simulation.

A lessons learned analysis was performed following the prototype construction and the beam test and is documented here [13]. The main conclusions are that first, the expected resolutions reported in the conceptual design report are ambitious. Second, a design iteration was required for the straw end pieces. Third, the resource estimates for the construction used in the basis of estimates were verified. However, the resource type was not. The BOEs at conceptual design relied mainly on student labor for construction. The prototype construction clearly demonstrated that either skilled technicians are required or several more hours would be required. All of the lessons learned are incorporated in the technical design.

The design of the tracker is driven by requirements for reducing systematic uncertainties on the $g-2$ measurement. However, by measuring the positron vertical angle, the tracker will also be able to limit the size of the muon's permanent electric dipole moment. Considering only the acceptance of the recommended design and requiring at least three stations are

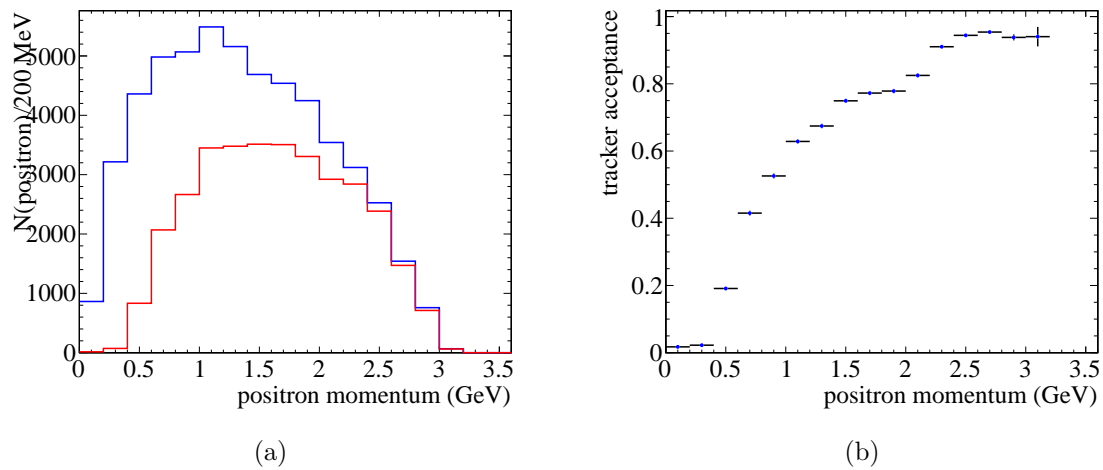


Figure 19.27: (a): The positron momentum spectrum for positrons incident on the front face of the calorimeter (blue) and also with sufficient hits in the tracking detector to form a track (red). (b): The ratio of the two distributions giving the relative efficiency between the tracker and the calorimeter as a function of positron momentum.

hit by the positron, we expect to increase the statistics with respect to the Brookhaven EDM search [2] by approximately a factor of 200 per month and a factor of 3500 for the full run. This gives us enough statistics to improve the limit on the EDM by an order of magnitude very quickly and eventually approach a two order of magnitude improvement assuming systematics can be properly constrained.

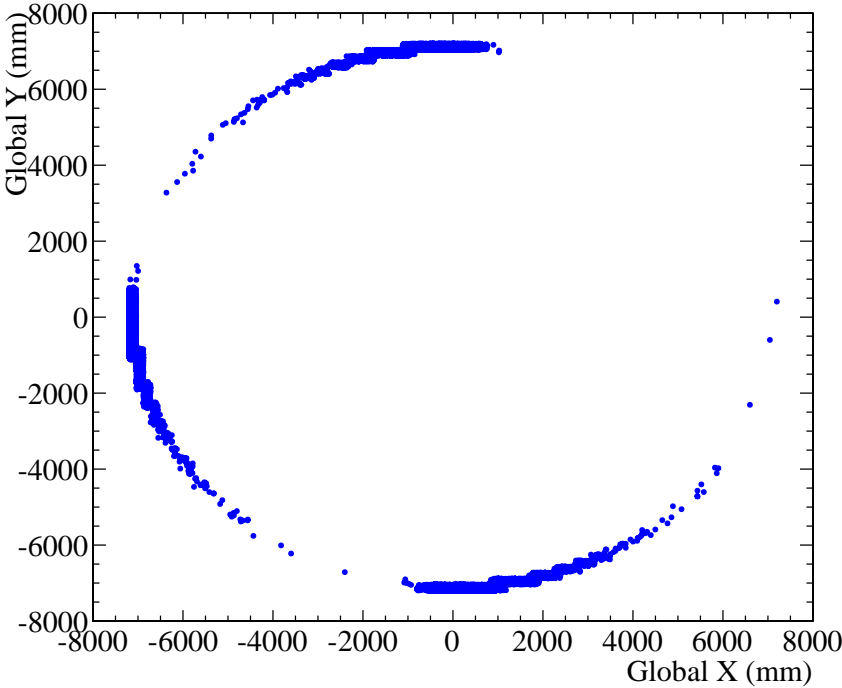


Figure 19.28: Azimuthal acceptance of the three trackers.

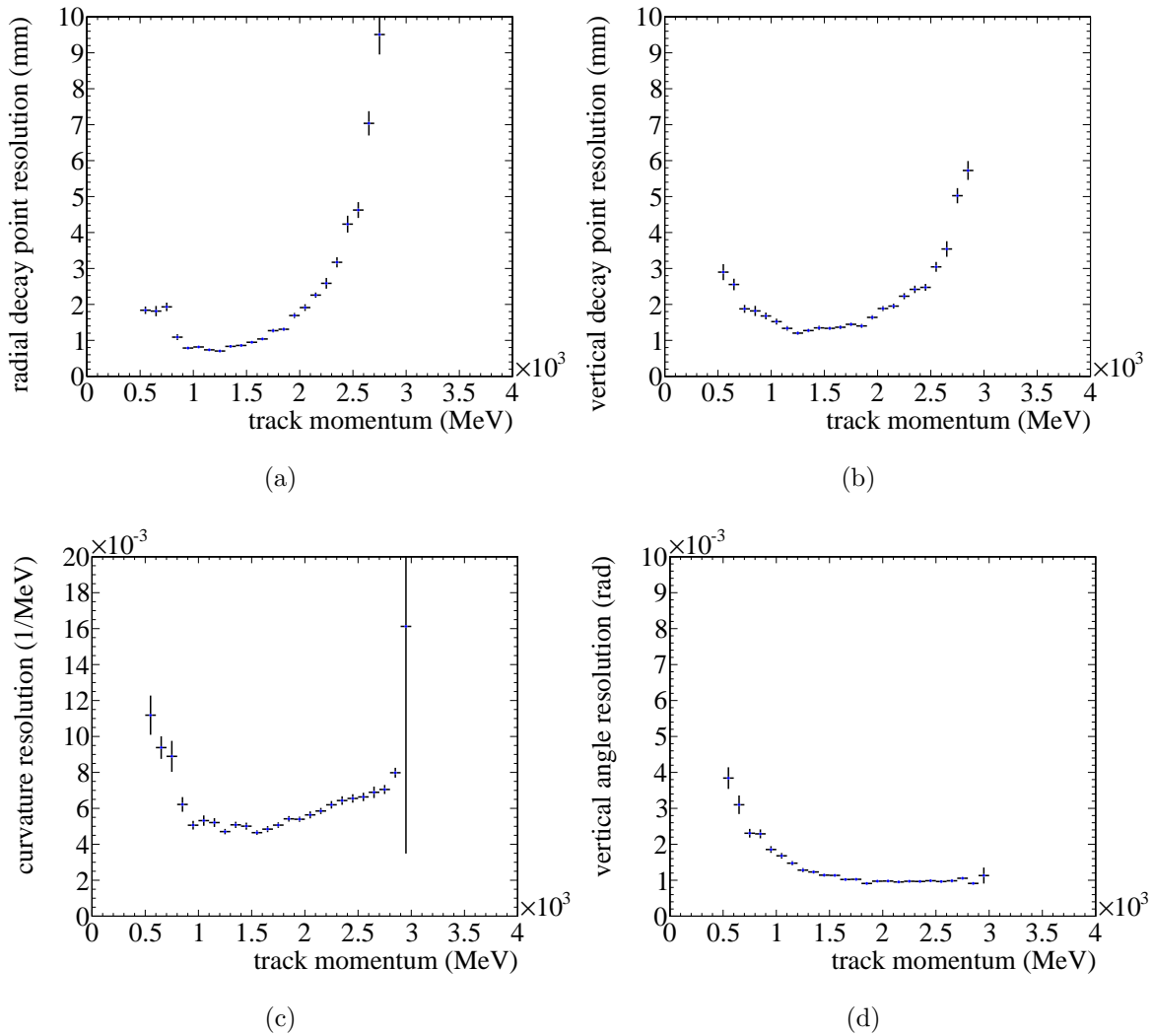


Figure 19.29: Resolutions on the muon and positron parameters that will be measured by the tracker. (a): The radial decay position of the muon. (b): The vertical decay position of the muon. (c): The curvature resolution of the positron. (d): The vertical angle of the positron.

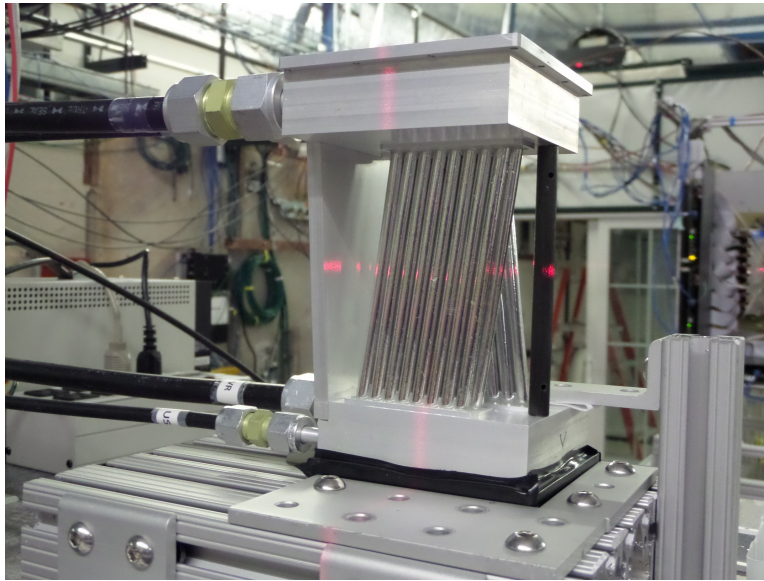


Figure 19.30: 32 channel prototype mounted in the Fermilab Test Beam Facility

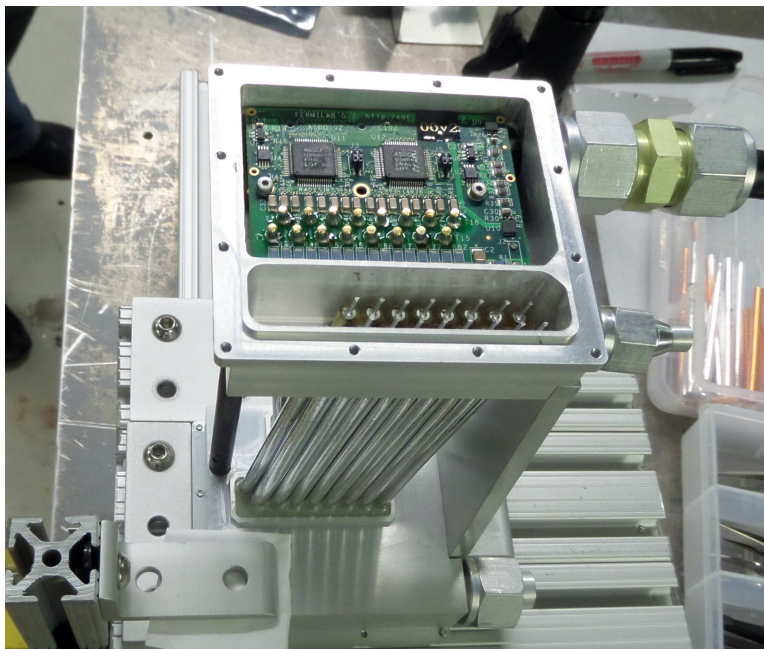


Figure 19.31: ASDQ boards mounted inside the manifold of the 32 channel prototype



Figure 19.32: 128 channel prototype mounted in the Fermilab Test Beam Facility

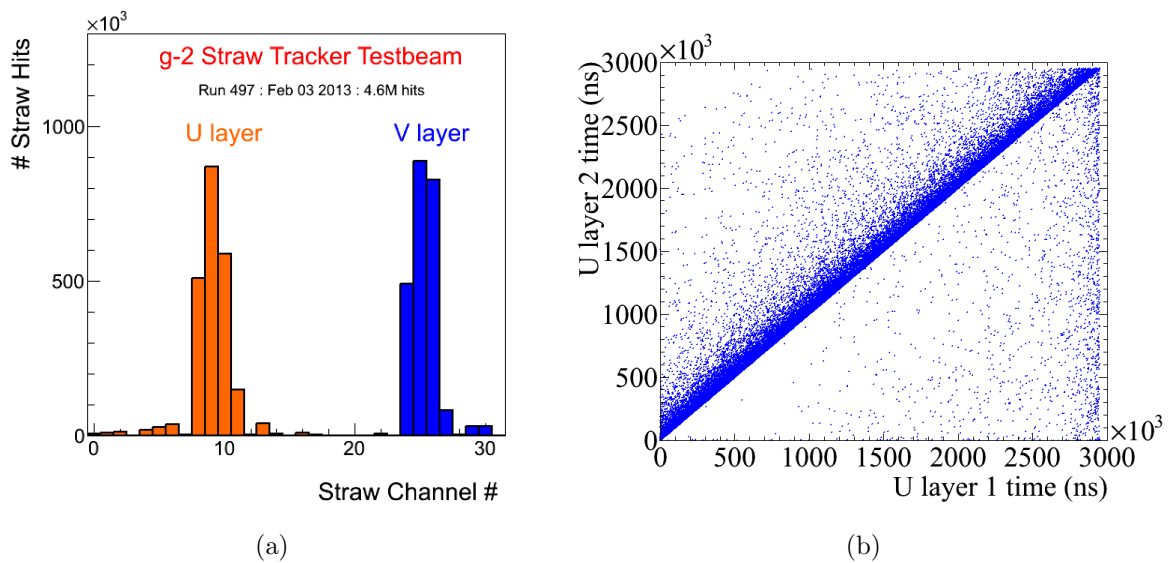


Figure 19.33: Data from the 32 channel prototype. (a): The hit distribution in channels showing the beam width and coincidences in the U and V layers. (b): The correlation between times in the two straw layers in the U view.

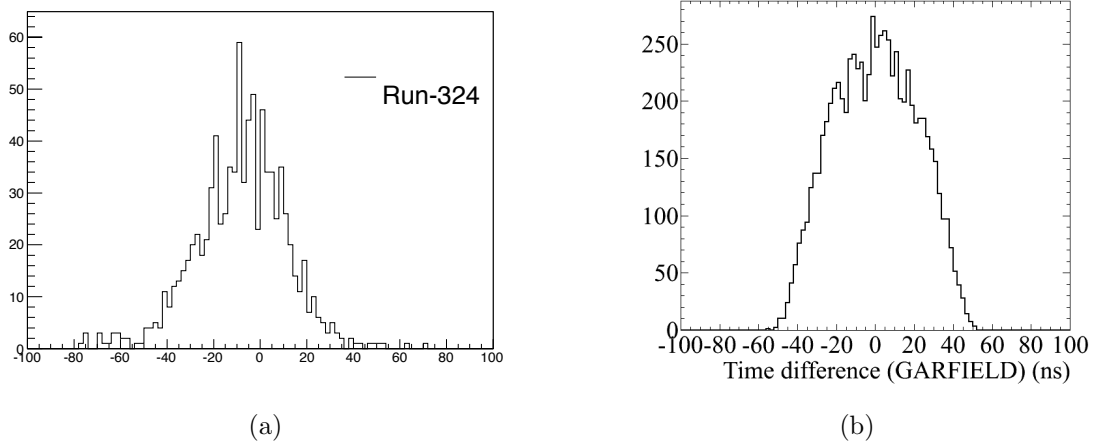


Figure 19.34: Time difference between hits in a straw doublet. The width of the distribution is determined by the straw diameter, drift velocity, and resolution. The distribution on the left is for data from the beam test. The distribution on the right is from GARFIELD after the effective threshold extracted from data has been applied.

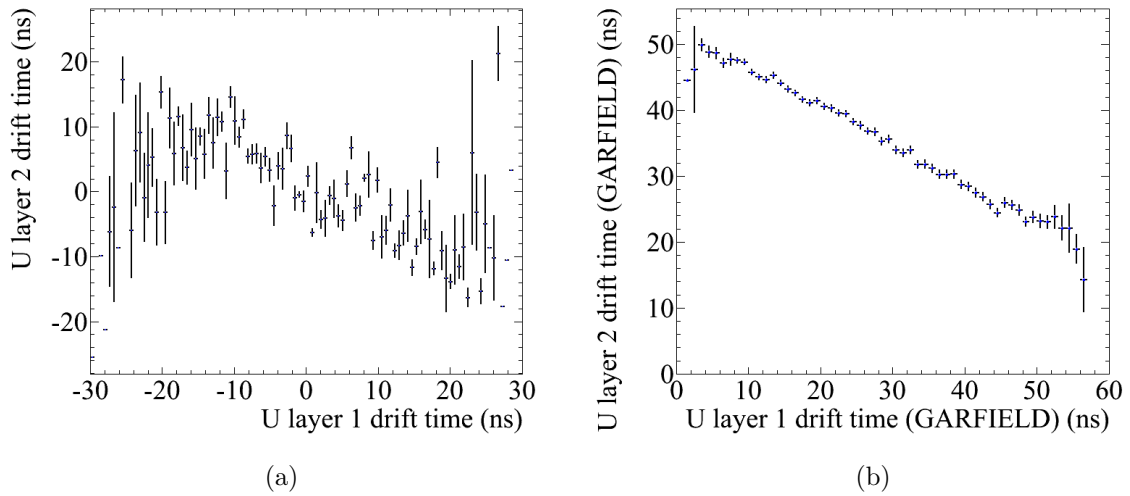


Figure 19.35: Anti-correlation between the drift times in the straw doublet. The distribution on the left is for data from the beam test. The distribution on the right is from GARFIELD after the effective threshold extracted from data has been applied.

19.5 Alternatives

The down selection of the preliminary design has been an evolving process. We are confident that after thoroughly exploring all the alternatives listed below, we have converged on an optimal solution given the requirements and constraints. There are alternatives, mainly regarding the mechanical connection of the straws to the readout electronics, that will be explored and settled prior to construction but we expect the main features to stay intact.

The two leading alternatives to a straw based system for the tracker are both silicon based. The first would use 300 μm Hamamatsu single sided strip sensors. These sensors were purchased for the DØ Run IIb detector upgrade [14] but never used. Sufficient sensors are in hand to build the $g - 2$ tracker. The readout would be based on the FSSRII chip [15] originally designed for BTeV and now being used for instrumentation upgrades for the JLab 12 GeV program. Tracking stations could be made with two sensors at a small stereo angle for a total material budget of 0.5% X_0 per station.

The second alternative would use the 50 μm thick Mimosa 26 pixel sensor [16] that has been developed with ILC R&D funding. There is about 25% dead space on the chip which would require a doublet structure to maintain adequate acceptance. Material is also needed in the active region for cooling and for flex cables. A thermal model of the device indicates that heat can be adequately dissipated if the two layers are mounted on blocks of 2.5 mm thick Si foam. After the Si foam and flex cables are added, the material budget is also close to 0.5% X_0 per station.

If we had a well defined interaction point and could build something like a 4 layer detector, either of these two alternatives would be preferable to straws. However, the DC nature of the beam requires us to have a multi layer device to sufficiently cover the momentum spectrum of the positrons. Building this out of the silicon options above would add far too much material and the effects of multiple scattering would severely compromise our ability to extrapolate the positron trajectories all the way back to the muon decay position.

For the amplifier, besides the ASDQ chip, we explored using discrete components or building an ASIC. Discrete components were ruled out due to space considerations and also due to power consumption. An ASIC is an expensive alternative particularly since the ASDQ chips are free, but it has the advantage that we could control all material used in the chip to avoid magnetic components such as tin. However we brought the ASDQ and FPGA chips to a 1.5 T test magnet at the Fermilab Technical division and determined that these chips have magnetic properties well within our specifications.

For the TDC, we considered commercially available products such as the 128 channel CAEN 767 or 1190 model multi hit TDCs. This would require bringing all signals out of the vacuum through some sort of feedthrough system. We investigated the feedthroughs being designed for liquid Argon TPC detectors that have the electronics placed inside the cryostat but these would have difficulty operating at the $g - 2$ vacuum of 10^{-6} Torr. The current design of an FPGA-based TDC is much more simple and cost effective.

For the electronics placement, we have considered designs with both the ASDQ and TDC boards inside the manifold (the conceptual design) as constructed for the 32 channel prototype, a design with both boards outside the manifolds (roughly equivalent to a design produced for Fermilab test beam wire chambers), and a design with the ASDQ boards inside the manifolds and the TDC boards outside the manifolds. The driving constraints are the

desire to place the ASDQ as close to the end of the straws as possible without generating excessive heat in the manifold that would require complicated cooling. From the lessons learned from building the 32 channel prototype and operating it in test beam conditions, it is clear that there is not sufficient overhead in signal to noise to allow for the analog signals to be brought outside of the manifold. However, once the signal is digitized there is no constraint on the distance between the ASDQ board and the TDC board. We therefore chose the design with the ASDQ board inside the manifold with modest cooling and the TDC boards outside the manifold. If future versions of the electronics or straw construction yield a higher signal to noise, the gain on the straws can be reduced which will help elevate any issues associated with aging or excessively high rates early in the fill.

For the backend electronics and low voltage distribution we have considered two alternatives. The first is a custom AMC card that acts as a link between the TDC and fronted DAQ that also incorporates the low voltage distribution to the electronics as outlined in the conceptual design. The second is the semi-commercial option of using the FC7 AMC board available from CERN that works readily with our μ TCA architecture and is essentially a large FPGA with configurable inputs and outputs. The low voltage would then be provided by commercial modules. This second choice was chosen since it involves significantly less engineering and provides a large amount of flexibility moving forward.

For the vacuum modifications, we have studied in detail three alternatives. First is a design that makes no chamber modifications and uses the existing ports upstream of the calorimeters. This is the least expensive solution but only allows us to build a tracker with approximately a 0.5 meter lever arm, greatly reducing the performance of the system. Second is a design that adds a flange to the vacuum chambers but maintains the vertical and radial dimensions of the chambers. This is a modest cost and allows for the maximum length for the tracker lever arm and was chosen as the conceptual design. However, the installation, plumbing, alignment, and reproducibility of placement all became serious issues with this design because it required the modules to be placed in the chamber, connections made between the modules and the flange, and finally mounting of the flange. The third design calls for radial extensions to the vacuum chamber that allow for an increase in the vertical size of the chamber. While the most expensive option, this allows modules to be mounted directly to the flange solving several engineering issues that arrived in the conceptual design and greatly reducing risks associated with alignment.

For the straw geometry, we have studied the performance as a function of straw pitch and naturally find the best performance for a pitch equal to the straw diameter. For the conceptual design, we chose a pitch of 5.5 mm. Finite element analysis indicated that this was the minimum pitch that could hold off the vacuum differential across the manifold wall with sufficient safety factor and without having an excessive manifold wall thickness. The 32 channel prototype was built with this pitch. It was found that with this pitch, a significant amount of post processing was required after the manifolds were removed from the CNC machine. The main issue is the relative softness of aluminum and the inability to hold proper tolerances between neighboring holes. We have therefore moved to a design that has a 6 mm pitch. This has been shown to make a major difference in terms of holding tolerances on the machined pieces greatly reducing the labor associated with construction while simulation indicates it is a marginal reduction in performance. Given the increased pitch, we also revisited the choice of doublet versus triplet straw configurations. While the

triplet has superior performance in terms of the information gained from a single module particularly if the track goes through a straw gap, the number of modules hit for each track is large enough to counter inefficiencies in a single module. The relatively small increase in performance contrasted with the 50% increase in both channel count and vacuum load lead us to retain the doublet configuration.

For the straw gas, we have studied Ar:CO₂ and Ar:Et. Using CO₂ as a quencher has the advantage of being non-flammable but has the disadvantage of only being able to operate at low gain. CO₂ also has the disadvantage of having a high permeation rate through Mylar. Ethane has excellent quenching properties and a 50:50 mixture of Ar:Et has excellent linearity properties. The two disadvantages are the mixture is flammable and a pure mixture has poor radiation tolerance leading to polymerization of the sense wire. We have now been able to construct a prototype system based on Fermilab ES&H document 6020.3 "Storage and Usage of Flammable Gas" and the prototype has passed an operational readiness review which gives us confidence that we can design a safe device. Since Ar:Et is a standard gas choice, particularly for straws, there are several well known additives that counter act the polymerization process and we have chosen per mil concentration of oxygen based on experience operating the CDF tracking detector. While CO₂ meets the requirement specifications, there is no headroom. Ethane as a quencher allows higher gain operation providing significant headroom. We have those chosen Ethane as a quencher.

19.6 ES&H

The $g-2$ tracker is similar to other gas-based detectors that are commonly used at Fermilab and the $g-2$ tracker is identical in many cases to the Mu2e system. The main hazard is flammable gas. The area around the tracker will be a class zero flammable area and the operating procedures in the Fermilab ES&H manual for storing and operating a flammable gas system will be followed. Other potential hazards include power systems and compressed gas. The gas will permeate at a small level inside the $g-2$ vacuum and come in contact with the quadrupole high voltage. Any gas leak in the experimental hall will also bring the gas in contact with the high voltage stand-offs and feed-throughs of the kicker and quadrupoles. Because of this, and because using non-flammable gas appears to satisfy the performance requirements, we are precluding the use of flammable gas. These and all other hazards have been identified and documented in the Muon $g-2$ Hazard Analysis [17].

The detector requires power systems with both low voltages with high currents and high voltages. During normal operation, the tracker will be inaccessible inside the storage ring. Power will be distributed to the tracker through shielded cables and connectors that comply with Fermilab policies. Fermilab will review the installation prior to operation.

Gas that will be used for the tracker will be kept in DOT compliant cylinders in quantities limited to the minimum required for efficient operation. The cylinders will be stored in a dedicated location appropriate to the type of gas being used. The storage area will be equipped with fire detection and suppression systems. The installation, including all associated piping and valves, will be documented and reviewed by the Fermilab Mechanical Safety Subcommittee.

The detector itself does not have any radioactive sources. However, Fe⁵⁵ sources will be

used to measure the gain of the straws before installation. Usage of radioactive sources will be reviewed to ensure adherence to Fermilab safety policy. In particular, the sources will be properly inventoried and stored and we see no opportunity for producing mixed waste.

Solvents such as ethanol will be used to clean components before assembly and epoxy resins will be used in the assembly process. All chemicals will be clearly labeled and stored in approved, locked storage cabinets and will adhere to the Fermilab safety policy.

19.7 Risks

19.7.1 Performance Risk

The tracker has been designed assuming a maximum instantaneous rate of 10 kHz/cm^2 . This value is extrapolated from measurements at the Brookhaven experiment. The Brookhaven experiment had significant contamination from pions that led to a large hadronic flash at the beginning of the fill. This pion contamination has been removed from the Fermilab experiment but there is still a possibility that there will be some unaccounted for background that leads to unacceptable rates. The straws have been designed to operate with CF_4 so a faster gas could be used to deal with this. We are also investigating using a circuit to reduce the gain of the straws during injection. This is complicated and would require electrical engineering resources to design if we are required implement this.

The system of collimators used to scrape the muon beam after injection is partially in the line of sight of the tracking detectors. This would limit the acceptance of the tracker and potentially cause high backgrounds early in the fill. To mitigate this risk, we are performing studies to determine alternative locations for the collimators and working closely with the groups associated with the collimator system.

19.7.2 Technical and Operational Risk

The greatest technical risk is that the tracking system will in some way affect the precision magnetic field of the storage ring. This risk is being mitigated in several ways:

- All scientists, engineers, technicians, students, and vendors involved in the design and construction of the system are educated on the importance of the magnetic properties of the system.
- The specifications are clearly stated in terms of the static and dynamic effects on the field. These have been documented and agreed on by the collaboration.
- Individual components are taken to an existing 1.5 T test magnet and their static magnetic properties are verified to be within specifications.
- Full magnetic simulation of the detector using OPERA [18] will be added to the existing storage ring OPERA simulation to verify that any static effects can be shimmed out of the field using the existing shimming kit.
- The full detector will be tested in a test solenoid that is being shipped from LANL to Fermilab specifically for this purpose.

- A fast coil will be designed to measure the size and time structure of any transient magnetic fields being produced by the electronics.

As discussed above, all prototype electronics constructed so far have been within the magnetic field specifications.

The vacuum specifications for the g-2 storage ring are set by the electrostatic quadrupoles inside the storage ring. The combination of the electric field from the quads and the magnetic field from the g-2 magnet leads to regions where photoelectrons can be captured in Penning traps. These electrons can eventually interact with residual gas molecules, leading to avalanche and sparking. This is the primary factor influencing the lifetime of the quadrupole plates.

For μ^+ operation, a vacuum of 10^{-6} Torr is required. If μ^- running is required or if the quadrupoles are operated at a greater HV to move to a different tune point, the vacuum may need to be improved to 10^{-7} Torr. The leak rate of the straws has been measured by Mu2e and indicates that 10^{-6} Torr can be achieved. To mitigate the risk of needing to operate at a higher vacuum we are designing the ability to add higher capacity to the pumping speed near the tracking detectors. We have also added a 25 μm secondary containment barrier using aluminized Mylar. This greatly increases the efficiency of any local pumping but adds material in front of the detector.

Contaminated gas is a serious risk for any drift chamber. This risk is mitigated in several ways. We will perform a detailed analysis on each batch of gas before it is incorporated into the system. Finally, spare chambers in test stands will use the same gas and will be illuminated with radioactive sources to monitor gain and give early warning of problems.

A broken wire will cause an entire plane of a module to be inoperable. A broken straw will cause an entire module to be inoperable. To mitigate this risk, the system is being designed in a way so that a damaged module can be easily removed and replaced with a spare with approximately 1 day lost to reestablishing the vacuum. We anticipate breaking vacuum at least once every several months to service the NMR trolley so as long as the frequency of problems is much less than this, there is no risk to the run schedule.

19.8 Quality Assurance

Proper quality assurance is essential to construct a tracking detector that meets the Muon $g - 2$ requirements for performance and reliable operation. Quality assurance will be integrated into all phases of the tracker work including design, procurement, fabrication, and installation.

Individual straws must be leak tight, straight, and be held at the proper wire tension. As the straw modules will be placed in vacuum, leak testing is essential to ensure that the vacuum in the region of the tracking stations is not unduly degraded. The straws will be leak tested before being installed. The straws will be connected to a clean gas system and over-pressured. The leak rate will be measured over an appropriate time interval by measuring the pressure drop. A leak/burst testing apparatus for a single straw has been constructed, as shown in Fig. 19.36. Based on experience with this testing apparatus, a new leak testing apparatus is being designed (see Fig. 19.36 for a design image) which can test multiple straws in parallel. After the assembly of a station, the entire station will be leak tested again. This

will be accomplished by placing the straw tube module into a vacuum chamber and flowing clean gas into the module while pumping down the chamber. The module leak rate will be measured by monitoring the pressure in the vacuum chamber versus time.

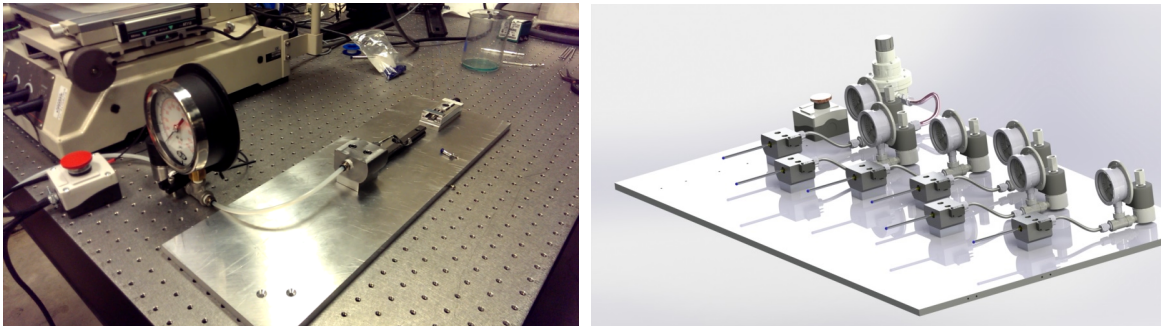


Figure 19.36: Photo of a single-straw leak testing/bursting test apparatus (left). Design drawing of a multiple straw leak testing apparatus (right).

The straws must maintain their shape and be mounted at the proper stereo angle to operate efficiently and to maintain an appropriate distance between the wire and the grounded Mylar surface to avoid breakdown. Straws will first be visually inspected for roundness and straightness before assembly. Flawed straws that escape detection during visual inspection can be identified by non-uniform gas gain and resolution. This will be done as part of the wire position measurement. In addition to visual inspection, the resistance of the straws will also be measured throughout the assembly process. The Mylar straws conduct through the few-hundred Angstrom aluminum and gold coatings. Our experience with these straws has shown that the resistance of the straws is very sensitive to physical damage to straws, likely through damage to the thin conductive coating [19].

The appropriate tension must be applied and maintained in a straw for efficient, stable operation. Tension is applied through calibrated mechanical force but can be lost through relaxation mechanisms. Additionally, since the straws are primarily composed of Mylar, when under tension they will experience a lengthening over time (referred to as "creep"). This creep effect will reduce the tension in the straw over time. Straw creep has been measured over a duration of approximately one year [19]. For the values of straw tension to be used in the modules, the amount of straw creep is negligible and not a concern.

Both wire and straw tension will be measured after assembly using vibrational resonance techniques appropriate to our short straws. Utilizing the experience of other experiments that have used straw tubes, testing procedures have been devised to measure both the straw tension and the wire tension after the straw tube modules have been assembled. These tests are detailed in Ref. [19] and Ref. [20]. Both tests are based on measuring the frequency of the induced EMF in a vibrating wire/straw in a magnetic field. Proof-of-principle tests have shown that the tension can be measured precisely enough for our needs. (Note that due to the short straws/wires and nearly vertical orientation, straw/wire sag is not a significant concern.)

All electronics components will be tested prior to installation on the tracking stations including a suitable burn-in period. The high voltage circuits will be tested for leakage

current. The threshold characteristics of each channel will be tested with a threshold scan. A noise scan will be performed for various threshold settings to identify channels with large noise fractions. The FPGA TDCs will be validated by comparing their output to commercial TDC devices with higher resolution. After the final assembly of a straw module (including the electronics), all modules will undergo a system test utilizing cosmic rays or a radioactive source to verify the operation and performance of all channels.

19.9 Value Management

The tracker technology for Muon $g - 2$ is well established and has been implemented in other high energy and nuclear physics experiments. Value management principles have been applied over time during the development of the technology. Value management moving forward is mainly related to labor costs since the straw tracker assembly will be labor intensive. We have identified collaborating institutions with the technical capabilities to perform a large fraction of the assembly work at minimal cost.

We are subcontracting engineering to university engineering departments and using Fermilab engineering resources to perform independent design reviews before production or procurement. This keeps the overall engineering costs low while maintaining the standards of Fermilab engineering.

The back-end readout electronics and data acquisition for the tracker are equivalent to those used for the calorimeters. This simplifies the design and operation of the system. However, once the final specifications are known, we will investigate possible cost savings by using different system components. Current FPGA technology is sufficient to meet the needs of the tracker electronics. These will be purchased once they are no longer the most current devices which should lead to significant cost savings. Sufficient spares will be purchased to ensure the stock for the lifetime of the experiment.

The straw terminations require injection molded pieces. The cost of these pieces is almost entirely driven by the cost of the mold and so design iterations are costly. To mitigate this, we intend to first produce all injection molded pieces with a 3-D printer and construct straws with the printed pieces to validate the design before the molds are procured.

References

- [1] G. W. Bennett *et al.* (Muon $g - 2$ Collaboration) Phys. Rev. D 73, 072003 (2006).
- [2] G. W. Bennett *et al.* (Muon $g - 2$ Collaboration) Phys. Rev. D 80, 052008 (2009).
- [3] B.C.K. Casey, D. Kawall *et al.* Field specification in preparation.
- [4] R.E.Ray, Mu2e-doc-1169-v21
- [5] S. Graessle *et al.*, Nucl. Inst. Meth. A 367, 138 (1995).
- [6] See for example R. Openshaw *et al.*, IEEE Trans. Nucl. Sci, 36, 567 (1989).
- [7] T. Affolder *et al.*, Nucl. Inst. Meth. A 526, 249 (2004).
- [8] E. Hazen *et al.* JINST 8 C12036 (2013).
- [9] <https://svnweb.cern.ch/trac/cactus/wiki> and “Update on IPBus v2”, Talk at the xTCA Interest group, CERN (2013)
<https://indico.cern.ch/event/237173/contribution/7/material/slides/0.pdf>
- [10] J. Troska *et al.*, IEEE Trans.Nucl.Sci., 3, 834 (2006).
- [11] The appropriate reference for Garfield.
- [12] S. Agostinelli *et al.* Nucl. Inst. Meth. A 506, 250 (2003).
- [13] B.C.K. Casey *et al.* GM2-doc-1634.
- [14] D. S. Denisov, S. Soldner-Rembold, Fermilab-Proposal-0925, Fermilab-Design-2001-02, (2001).
- [15] R. Yurema *et al.*, IEEE 52, 799 (2005).
- [16] R. De Masi *et al.*, PoS (HEP-EPS 2009), 157 (2009).
- [17] K. W. Merrit. Hazard analysis document in preparation.
- [18] OPERA. Cobham Technical Services, Vector Fields Software, 1984-2012.
- [19] M. Eads, A. Epps, O. Escalante-Aguirre, and M. Shenk, GM2-doc-1926-v1.
- [20] M. Eads. O. Escalante-Aguirre, GM2-doc-1927-v1.

